Studies and Optimization of All-Polymer Solar Cells based on Naphthalene Diimide-Biselenophene Copolymer Acceptors

Hyunjong Lee

A thesis

submitted in partial fulfillment of the

requirements for the degree of

Master of Science in Chemical Engineering

University of Washington

2018

Committee:

Samson A. Jenekhe

Qiuming Yu

Program Authorized to Offer Degree:

Department of Chemical Engineering

University of Washington

Abstract

Studies and Optimization of All-Polymer Solar Cells based on Naphthalene Diimide-Biselenophene Copolymer Acceptors

Hyunjong Lee

Chair of the Supervisory Committee:
Samson A. Jenekhe
Department of Chemical Engineering

Enormous progress has been made in the field of organic photovoltaics (OPVs) for future energy applications in the last two decades. Studies and understanding of fullerene-based polymer solar cells have led to a power conversion efficiency (PCE) of over 12%. However, such fullerene-based OPVs are not stable in air, among other disadvantages. This thesis mainly focuses on studies all-polymer solar cells (all-PCSs) based on naphthalene diimide-biselenophene copolymer acceptors and aims to better understand the relationship between photovoltaic properties, blend morphology, and device processing variables.

In this study, we found that optimal thermal annealing and use of a processing additive facilitated favorable blend morphology and enhanced photovoltaic properties in an active layer

composed of a high molecular weight (M_n) acceptor polymer, PNDIBS, and a donor polymer, PBDB-T, with complementary absorption bands. We observed a PCE of over 9% in optimized PBDB-T:PNDIBS blend devices. In addition, all-PCSs based on donor PBDB-T and random copolymer acceptors, BSS*x* (*x*=10, 20, and 50), were found to have improved morphology, due to the fine tuned bulk crystallinity of the random copolymers. Finally, we explored solution-processed electron transport layers (ETLs) as a way to engineer the cathode interface of the all-PCSs and found that ETLs doped with alkali metal salt can also further enhance the device performance due to the better charge extraction at the cathode.

TABLE OF CONTENTS

LIST OF FIGURES

LIST OF TABLES

ACKNOWLEDGEMENTS

I sincerely wish to express my gratitude to Professor Samson A. Jenekhe, my MS thesis advisor, for his guidance and support. His insightful comments and suggestions have been indispensable to the completion of my research, and his valuable life advices has helped me to grow into a better person. I also appreciate Professor Qiuming Yu for their time serving on my committee and for providing valuable suggestions.

I would like to thank the following past and present members of the Jenekhe research group: Dr. Robert Ireland, Dr. Selvam Subramaniyan, Dr. Nagesh B. Kolhe, Xiaomei Ding, Yuwei Chen, Mary Nguyen, Yuyan Zhu, Duyen K. Tran, Sarah Marie West, Jiangtian Zhang. They have influenced my research and life through insightful discussions, successful collaborations, encouraging each other and sharing happy moments.

I would like to acknowledge the Department of Chemical Engineering at UW, the National Science Foundation, the Office of Naval Research for financial support of different parts of this research.

Finally, I would like to express my gratitude and love for my parents, my sisters, and my friends. Without their support and encouragement, this work would not have been possible.

Chapter 1. INTRODUCTION

1.1 BACKGROUND

Since conducting polymers discovered in 1977, organic photovoltaics (OPVs), one of a representative application in organic electronics and photonics, have attracted great attention and developed due to their advantages of mechanical properties (lightweight, flexibility, and transparency) and low cost solution processibility in large scale as next-generation light harvesting technology.[1–3]

Specifically, extensive studies and efforts have been focused on developing fullerene-based polymer solar cells in bulk heterojunction structure where electron-accepting semiconductors (*n*-type) and electron-donating semiconductors (*p*-type) are blended by forming an interpenetrating network. However, some drawbacks (costly synthesis, limited absorption in the visible range, limited chemical and energetic tunability, and poor stability) of fullerene derivatives with existing abundant and various p-type polymers have raised up the development of all-polymer solar cells (all-PSCs). Although limited studies and optimization of devices have conducted in all-PSCs due to the scarcity of n-type polymer semiconductors, all-PSCs have relative benefits of thermal, mechanical, and photostability as compared to fullerene-based polymer solar cells. Thus, a new development of n-type polymer semiconductors and their optimization for all-PSCs is of great interest in the field of OPVs.[4–7]

1.2 ORGANIC PHOTOVOLTAICS

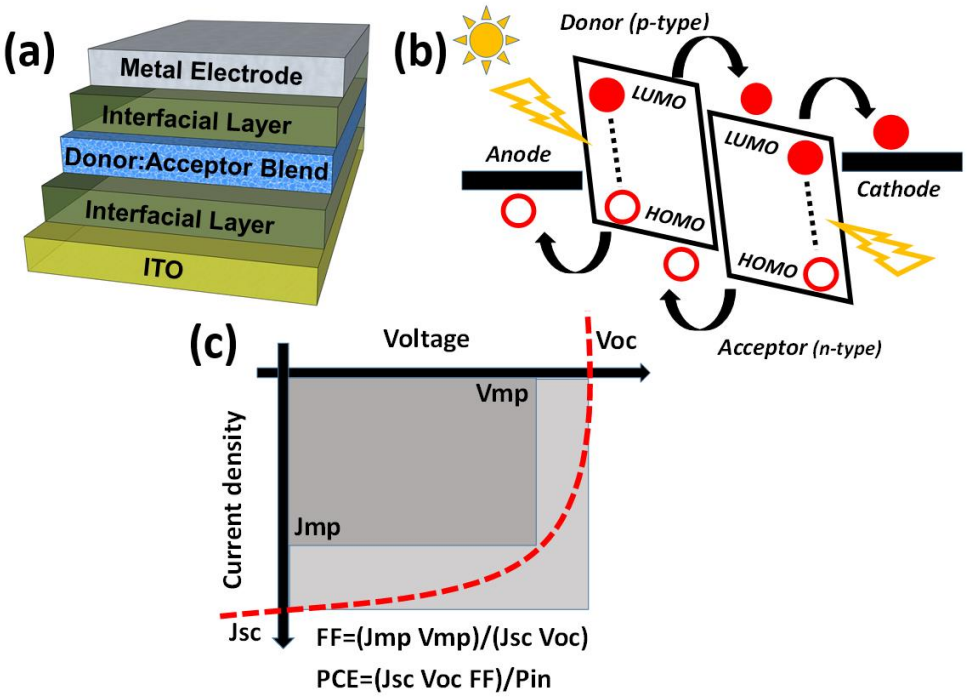

Figure 1. (a) Basic OPV device structure. (b) Basic operation mechanism of OPVs. (c) Typical current density (J_{sc}) – Voltage (V) characteristics of OPVs under illumination.

Organic photovoltaics (OPVs) (or organic solar cell) is one of great interest in the field of renewable energy and various applications required to use electricity. Although the power conversion efficiency (PCE) is much lower than inorganic solar cells, which can be used in solar energy generation, it is worth to put considerable efforts on developing OPVs due to the advantages of lightweight, flexibility, and low-cost processing for commercial applications.

As shown in Figure 2 (a), OPVs consist of various layers to maximize the device performance. On the basis of the active layer where donor and acceptor organic semiconductors are blended, each interfacial layer and electrode for electron and hole transport form layered device structure. For the operation of OPVs shown in Figure 2 (b), four steps (i) absorption photons and

exciton generation, (ii) exciton diffusion and dissociation, (iii) charge transfer, (iv) charge carriers collection are required. To be specific, an absorbed photon with larger energy than E_g of organic semiconductors in the active layer can form exciton as a form of an electron-hole pair. When this exciton diffuses to the donor/acceptor interface in the active layer, HOMO/LUMO energy difference can drive the exciton dissociated to charges (electron and hole) and transferred. Separated electron and hole is finally transported through interfacial layers and collected at the anode and cathode respectively.

To understand photovoltaic properties and determine the PCE($= \frac{J_{sc} * V_{oc} * FF}{P_{in}}$) of OPVs, it is required to analyze the important parameters (short-circuit current (J_{sc}), open-circuit voltage (V_{oc}), and fill factor (FF)) by drawing *J*-*V* curve (Figure 2 (c)). Finally, the optimization of OPVs is an important step to achieve high performance for future commercialization and their application. For the improvement, it is necessary to understand each role of layers and their interactions between them. In the case of the active layer, their broad range light harvesting should be maximized, and the film morphology should be explored to minimize recombination process, which can hinder the photovoltaic effect in organic blends. Furthermore, each interlayer and electrode should be studied for efficient charge collection and device stability.

1.3 DEVICE ENGINEERING FOR OPTIMIZATION

There are many factors which can affect OPVs performance. Mainly, it can be divided into two categories: molecular design and device engineering. In the perspective of molecular design, a molecular structure with different monomers, molecular weight, side chains, conjugation length, and purity can decide material properties such as energy level, optical property, crystallinity, charge transport property, and solubility. On the other hand, device engineering could be a

different story for OPVs. In the given blend of n-type and p-type organic semiconductors as bulk heterojunction structure, optimization of film morphology and maximization of charge collection are essential processes for enhanced device performance. To control the film morphology in solution processing, processing solvent and processing additives should be considered. Different solubility for donor and acceptor and their evaporation rate can affect the morphology of the film. Furthermore, processing conditions such as thermal annealing with different temperature and time or aged processing without thermal effect are another key factors for the blend kinetics and morphology. Also, various interlayers can affect the device performance by changing the work function of each electrode, forming interface molecular dipoles, and improving surface morphology with reduces contact resistance.

1.4 Major Challenges and Research Objective

1.4.1. Major Challenges

In the last few decades, the growing demand for renewable energy sources has accelerated to the development in photovoltaic (PV) field. Among various PV technologies, OPVs has attracted great attention due to the critical advantages such as lightweight, flexibility, cost-effective solution processability with extensive studies and development of various polymer semiconductors and organic electronic devices. First, most high-performance OPVs has developed from fullerene-based system polymer solar cell with a maximum PCE over 11%. For this moment, design and synthesis of new p-type polymer semiconductors for maximizing fullerene-based polymer solar cell was the main goal. However, the limitations of fullerene such as weak absorption in the visible region, difficulty in tuning optical and electronic properties, poor photostability started to develop new nonfullerene device system.

Although one promising system is an all-polymer system where the n-type polymer and p-type polymer semiconductor are blended, the scarcity of n-type polymer has limited the development of the all-PSCs. Currently, most all-PSCs studies have been done with naphthalene diimide-bithiophene copolymer acceptor also known as N2200, which shows high electron mobility, high electron affinity, good solubility, and strong absorption in the visible and near-infrared region.[8,9] At this moment, exploring the all-PSCs with new n-type polymer semiconductors and their various photovoltaic properties, blend morphology are required. Also, since interlayers can play an important role in the performance of OPVs, development of new electron-transport layers or hole-transport layers is necessary for the progress of OPVs.

1.4.2. Research Objectives

The primary objective of this research is to optimize the device processing, morphology and cathode interlayer of the all-polymer solar cell. The main focus is to address current scientific and technical challenges in the field. The specific scope of the research includes:

Optimization of all-polymer solar cells based on Naphthalene diimide-biselenophene copolymer acceptor with an understanding of photovoltaic properties and blend morphology. In Chapter 1, with optimal pairing with proper donor polymer (PBDB-T) which have complementary absorption with NDI-biselenophene copolymer (PNDIBS) as an acceptor, systematical optimization for all-PCSs with low-M_n (LP) and high-M_n PNDIBS (HP) acceptor polymers are presented. While LP is optimized with film aging process, HP shows the best performance with thermal annealing (150 ℃). Moreover, both LP and HP cases presented enhancement in photovoltaic properties with the addition of processing additive of DPE. In

addition to photovoltaic properties, surface and blend morphology will be discussed with surface roughness, molecular orientation, crystalline ordering, domain size.

Studying all-polymer solar cells with Naphthalene diimide-biselenophene random copolymer acceptor. In Chapter 3, NDI-biselenophene random copolymers (BSS10, BSS20, and BSS50) as a new n-type polymer semiconductor were explored in all-PSCs and discussed with their photovoltaic properties and blend morphology. Relative simple processing condition with thermal stability and without any processing additives are advantages of this blend system. As increasing the percent of selenophene, the change of photovoltaic properties was observed due to the transition of bulk crystallinity, which observed in GIWAXS data analysis. This results could open the path of new n-type polymer semiconductors with an understanding of controlling the bulk crystallinity for high-performance all-PCSs.

Engineering the cathode interface for enhancement of all-polymer solar cells. For enhancement in device performance of all-PCSs, electron-transport layer (ETL) has a significant role. ETL can affect the device stability, altering work-function of the electrode, passivation of traps, blocking hole transport and stimulating electron transport, and protection from metal diffusion. Also, solution processable ETL are beneficial in the aspect of cost and energy for making devices. In Chapter 4, various cathode cases were tested with analysis of photovoltaic properties based on BPhen, BmPyPhB, and TmPyPB as electron transport material with alkali metal salt dopant. Solution-processed ETLs showed superior improvement in photocurrent compared to other cathode cases, but reduced fill factor also was observed, which should be solved for the overall improvement of power conversion efficiency.

1.5 REFERENCES

(1) Chiang, C. K.; Fincher, C. R.; Park, Y. W.; Heeger, A. J.; Shirakawa, H.; Louis, E. J.; Gau, S. C.; MacDiarmid, A. G. Electrical Conductivity in Doped Polyacetylene. *Phys. Rev. Lett.* **1977**, *39* (17), 1098–1101.

(2) Forrest, S. R.; Thompson, M. E. Introduction: Organic Electronics and Optoelectronics. *Chem. Rev.* **2007**, *107* (4), 923–925.

(3) Brédas, J.-L.; Norton, J. E.; Cornil, J.; Coropceanu, V. Molecular Understanding of Organic Solar Cells: The Challenges. *Acc. Chem. Res* **2009**, *42* (11).

(4) Zhou, N.; Facchetti, A. Naphthalenediimide (NDI) Polymers for All-Polymer Photovoltaics. *Mater. Today* **2018**, *21* (4), 377–390.

(5) Huang, Y.; Kramer, E. J.; Heeger, A. J.; Bazan, G. C. Bulk Heterojunction Solar Cells: Morphology and Performance Relationships. *Chem. Rev.* **2014**, *114* (14), 7006–7043.

(6) Lu, L.; Zheng, T.; Wu, Q.; Schneider, A. M.; Zhao, D.; Yu, L. Recent Advances in Bulk Heterojunction Polymer Solar Cells. **2015**.

(7) Zhan, C.; Zhang, X.; Yao, J. New Advances in Non-Fullerene Acceptor Based Organic Solar Cells. *RSC Adv.* **2015**, *5* (113), 93002–93026.

(8) Yan, H.; Chen, Z.; Zheng, Y.; Newman, C.; Quinn, J. R.; Dötz, F.; Kastler, M.; Facchetti, A. A High-Mobility Electron-Transporting Polymer for Printed Transistors. *Nature* **2009**, *457* (7230), 679–686.

(9) Fabiano, S.; Himmelberger, S.; Drees, M.; Chen, Z.; Altamimi, R. M.; Salleo, A.; Loi, M. A.; Facchetti, A. Charge Transport Orthogonality in All-Polymer Blend Transistors, Diodes, and Solar Cells. *Adv. Energy Mater.* **2014**, *4* (6), 1–7.

(10) Courtright, B. A. E.; Jenekhe, S. A. Polyethylenimine Interfacial Layers in Inverted Organic

Photovoltaic Devices : Effects of Ethoxylation and Molecular Weight on E Ffi Ciency and Temporal Stability. **2015**, 1–5.

(11) Chen, L. M.; Xu, Z.; Hong, Z. R.; Yang, Y. Interface Investigation and Engineering - Achieving High Performance Polymer Photovoltaic Devices. *J. Mater. Chem.* **2010**, *20* (13), 2575–2598.

(12) Steim, R.; Kogler, F. R.; Brabec, C. J. Interface Materials for Organic Solar Cells. *J. Mater. Chem.* **2010**, *20* (13), 2499.

(13) Yi, C.; Hu, X.; Gong, X.; Elzatahry, A. Interfacial Engineering for High Performance Organic Photovoltaics. *Mater. Today* **2016**, *19* (3), 169–177.

(14) Zeng, H.; Zhu, X.; Liang, Y.; Guo, X. *Interfacial Layer Engineering for Performance Enhancement in Polymer Solar Cells*; 2015; Vol. 7.

(15) Duan, C.; Zhang, K.; Zhong, C.; Huang, F.; Cao, Y. Recent Advances in Water/Alcohol-Soluble π-Conjugated Materials: New Materials and Growing Applications in Solar Cells. *Chem. Soc. Rev.* **2013**, *42* (23), 9071–9104.

(16) Yang, T.; Wang, M.; Duan, C.; Hu, X.; Huang, L.; Peng, J.; Huang, F.; Gong, X. Inverted Polymer Solar Cells with 8.4% Efficiency by Conjugated Polyelectrolyte. *Energy Environ. Sci.* **2012**, *5* (8), 8208.

(17) Hu, Z.; Zhang, K.; Huang, F.; Cao, Y. Water/Alcohol Soluble Conjugated Polymers for the Interface Engineering of Highly Efficient Polymer Light-Emitting Diodes and Polymer Solar Cells. *Chem. Commun.* **2015**, *51* (26), 5572–5585.

(18) Li, C.; Schwab, M.; Zhao, Y.; Chen, L.; Bruder, I.; Münster, I.; Erk, P.; Müllen, K. A Phenanthroline Derivative as Exciton Blocking Material for Organic Solar Cells. *Dye. Pigment.* **2013**, *97* (1), 258–261.

(19) Liu, X.; Wu, Y.; Li, X.; Zhang, W.; Zhao, L.; Wang, H. Q.; Fang, J. CdS-Phenanthroline Derivative Hybrid Cathode Interlayers for High Performance Inverted Organic Solar Cells. *J. Mater. Chem. A* **2015**, *4* (1), 297–302.

(20) Chang, C. C.; Lin, C. F.; Chiou, J. M.; Ho, T. H.; Tai, Y.; Lee, J. H.; Chen, Y. F.; Wang, J. K.; Chen, L. C.; Chen, K. H. Effects of Cathode Buffer Layers on the Efficiency of Bulk-Heterojunction Solar Cells. *Appl. Phys. Lett.* **2010**, *96* (26), 94–97.

(21) Farinhas, J.; Ferraria, A. M.; do Rego, A. M. B.; Morgado, J.; Charas, A. Understanding the Role of Phenanthroline as Interlayer in Bulk Heterojunction Organic Photovoltaic Cells. *ChemistrySelect* **2016**, *1* (18), 5638–5646.

(22) Earmme, T.; Jenekhe, S. A. High-Performance Multilayered Phosphorescent OLEDs by Solution-Processed Commercial Electron-Transport Materials. *J. Mater. Chem.* **2012**, *22* (11), 4660–4668.

(23) Earmme, T.; Jenekhe, S. A. Improved Electron Injection and Transport by Use of Baking Soda as a Low-Cost, Air-Stable, n-Dopant for Solution-Processed Phosphorescent Organic Light-Emitting Diodes. *Appl. Phys. Lett.* **2013**, *102* (23).

(24) Earmme, T.; Jenekhe, S. A. Solution-Processed, Alkali Metal-Salt-Doped, Electrona Transport Layers for High-Performance Phosphorescent Organic Light-Emitting Diodes. *Adv. Funct. Mater.* **2012**, *22* (24), 5126–5136.

(25) Ahmed, E.; Earmme, T.; Jenekhe, S. A. New Solution-Processable Electron Transport Materials for Highly Efficient Blue Phosphorescent OLEDs. *Adv. Funct. Mater.* **2011**, *21* (20), 3889–3899.

(26) Huang, L.; Cheng, X.; Yang, J.; Zhang, L.; Zhou, W.; Xiao, S.; Tan, L.; Chen, L.; Chen, Y. High-Performance Polymer Solar Cells Realized by Regulating the Surface Properties of

PEDOT:PSS Interlayer from Ionic Liquids. *ACS Appl. Mater. Interfaces* **2016**, *8* (40), 27018–27025.

(27) Mengistie, D. A.; Ibrahem, M. A.; Wang, P. C.; Chu, C. W. Highly Conductive PEDOT:PSS Treated with Formic Acid for ITO-Free Polymer Solar Cells. *ACS Appl. Mater. Interfaces* **2014**, *6* (4), 2292–2299.

(28) Walzer, K.; Männig, B.; Pfeiffer, M.; Leo, K. Highly Efficient Organic Devices Based on Electrically Doped Transport Layers. *Chem. Rev.* **2007**, *107* (4), 1233–1271.

(29) Zhao, Z.; Wu, Q.; Xia, F.; Chen, X.; Liu, Y.; Zhang, W.; Zhu, J.; Dai, S.; Yang, S. Improving the Conductivity of PEDOT:PSS Hole Transport Layer in Polymer Solar Cells via Copper(II) Bromide Salt Doping. *ACS Appl. Mater. Interfaces* **2015**, *7* (3), 1439–1448.

(30) Huang, L.; Cheng, X.; Yang, J.; Zhang, L.; Zhou, W.; Xiao, S.; Tan, L.; Chen, L.; Chen, Y. High-Performance Polymer Solar Cells Realized by Regulating the Surface Properties of PEDOT : PSS Interlayer from Ionic Liquids. **2016**.

(31) Mcgillivray, D.; Thomas, J. P.; Abd-ellah, M.; Heinig, N. F.; Leung, K. T. Performance Enhancement by Secondary Doping in PEDOT:PSS/ Planar-Si Hybrid Solar Cells. **2016**, 6–11.

(32) Fan, B.; Ying, L.; Wang, Z.; He, B.; Jiang, X.-F.; Huang, F.; Cao, Y. Optimisation of Processing Solvent and Molecular Weight for the Production of Green-Solvent-Processed All-Polymer Solar Cells with a Power Conversion Efficiency over 9%. *Energy Environ. Sci.* **2017**, *10* (5), 1243–1251.

(33) Mihailetchi, V. D.; Xie, H.; De Boer, B.; Koster, L. J. A.; Blom, P. W. M. Charge Transport and Photocurrent Generation in Poly(3-Hexylthiophene): Methanofullerene Bulk-Heterojunction Solar Cells. *Adv. Funct. Mater.* **2006**, *16* (5), 699–708.

(34) Fan, B.; Ying, L.; Zhu, P.; Pan, F.; Liu, F.; Chen, J.; Huang, F.; Cao, Y. All-Polymer Solar Cells Based on a Conjugated Polymer Containing Siloxane-Functionalized Side Chains with Efficiency over 10%. *Adv. Mater.* **2017**, *29* (47), 1–7.

(35) Hwang, Y.; Courtright, B. A. E.; Ferreira, A. S.; Tolbert, S. H.; Jenekhe, S. A. 7 . 7 % Effi Cient All-Polymer Solar Cells. **2015**, 4578–4584.

Chapter 2. INVERTED ALL-POLYMER SOLAR CELLS:BLEND MORPHOLOGY AND OPTIMAL PHOTOVOLTAIC PROPERTIES

2.1 INTRODUCTION

All-polymer solar cells (all-PSCs), in which the active layer is composed of a hole-conducting (donor) polymer and an electron-conducting (acceptor) polymer, are technologically attractive alternatives to fullerene-based polymer solar cells.[1-7] Their enhanced light-harvesting properties, greater tunability of the molecular and electronic structures, and enhanced thermal and mechanical robustness mean that all-PSCs have the potential to be readily optimized and manufactured on a large scale.[6,8,9] Although considerable progress has been made in the last 5 years, raising the power conversion efficiency (PCE) of all-PSCs from under 3% to the current 8-10% range,[6, 10-15] this performance remains below that of the best fullerene/polymer devices (10-12%)[16-18] and predicted theoretical device efficiency[19, 20] of organic photovoltaics. In general, the key photovoltaic parameters — photocurrent and fill factor — remain relatively low even for the best all-PSCs reported to date[12-15] while open circuit voltage (V_{0c}) or optical bandgap (E_g^{opt}) energy loss ($E_{loss} = E_g^{opt}$-eV_{oc}) remains an important limitation in these devices.

Recent advances in the performance of all-PSCs have come from studies of only a few acceptor polymers.[4] Indeed, nearly all reports of all-PSCs with a PCE of about 8% or higher have been based on the extensively studied naphthalene diimide (NDI)-bithiophene copolymer (P(NDI2OD-T2) or N2200)[11-13] and its terpolymer derivatives.[14] The few exemptions include perylene diimide vinylene copolymers[15] and NDI-selenophene copolymer (PNDIS-HD).[6] Interestingly, although high field-effect electron mobility has been reported for NDI-biselenophene copolymer (PNDIBS),[21] the selenophene analogue of N2200, all-PSCs made from

it have so far had poor efficiency (PCE < 1%).[22, 23] In our earlier study, PNDIBS with 2-decyltetradecyl chains was paired with regioregular poly(3-hexylthiophene) (P3HT), resulting in all-PSCs with a PCE of 0.9%.[22] In a more recent study by others, PNDIBS with 2-octyldodecyl side chains and a low molecular weight (M_n = 43.1 kDa) was paired with a benzodithiophene-thienopyrroledione copolymer (PTP8) donor to achieve all-PSCs with a PCE of only 0.9%.[23] Thus, PNDIBS remains to be fully explored as an acceptor polymer for developing highly efficient all-PSCs.

In this Chapter, I report the synthesis and characterization of high molecular weight PNDIBS bearing 2-octyldodecyl side chains and its use as an electron-conducting polymer to develop high performance all-PSCs. We selected the donor polymer PBDB-T (also known as PCE12),[24, 25] whose molecular structure is shown in Figure 2a, to investigate the photovoltaic properties of PNDIBS in all-PSCs. Absorption spectrum of the medium bandgap (E_g = 1.80 eV) PBDB-T donor is seen to be perfectly complementary to that of the PNDIBS acceptor (Figure 2b), unlike the donor polymers used in the prior studies.[22, 23] The donor/acceptor energy level offsets of the PBDB-T/PNDIBS pair (Figure 2c) are also ideal for achieving efficient charge transfer and separation.[26] Inverted all-PSCs fabricated from binary blends of high molecular weight PNDIBS with PBDB-T were found to have a PCE of up to 9.4% with a high short circuit current density (J_{sc}) of 18.32 mA/cm^2. These results are among the highest observed so far in all-PSCs.[11-14, 27]

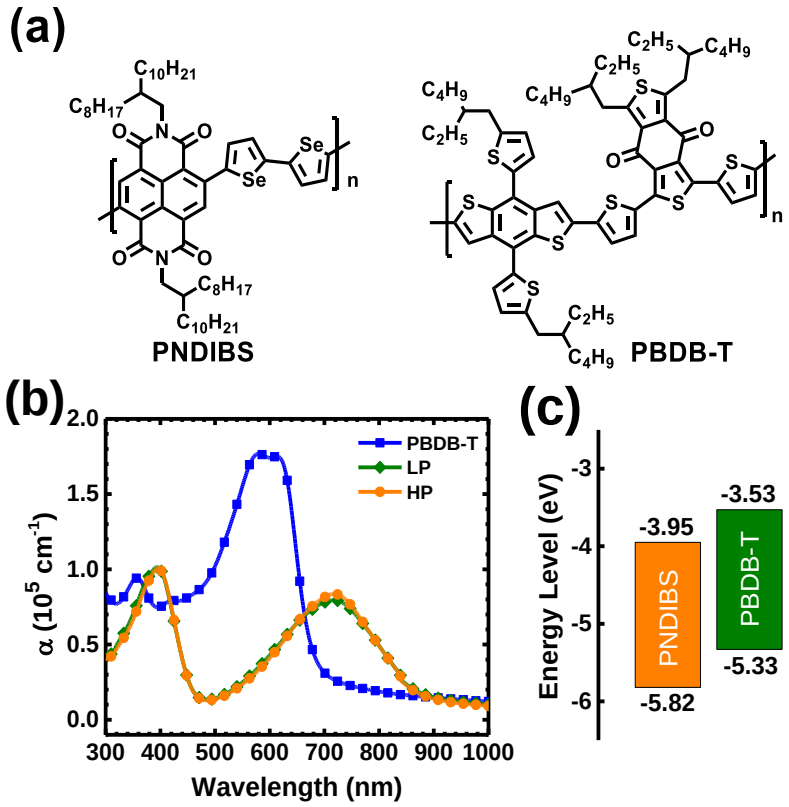

Figure 2. (a) Molecular structures of acceptor polymer PNDIBS and donor polymer PBDB-T. (b) thin-film optical absorption spectra of the acceptor and donor polymers. (c) HOMO/LUMO energy levels of the acceptor and donor polymers.

2.2 Experiment Section

Materials. Tri-(*o*-tolyl)-phosphine, tris(dibenzylideneacetone)dipalladium (0) ($Pd_2(dba)_3$), selenophene, trimethyltin chloride (20% solution) in THF, anhydrous copper(II)chloride, *n*-butyl lithium (2M in hexane), and chlorobenzene were purchased from Sigma-Aldrich and used without further purification. 5,10-Dibromoisochromeno[6,5,4-*def*] isochromene-1,3,6,8(*3aH, 8aH*)-tetraone and 2-octyldodecyl amine were purchased from Suna Tech Inc (Jaiansu, China). The donor polymer PBDB-T (M_n = 62 kDa, $Đ$ = 1.90) was purchased from Brilliant Matters Organic electronics (Quebec, Canada) and was used as received.

Monomer Synthesis. 5,5′-Bis (trimethylstannyl)-2,2’-biselenophene and 4,9-dibromo-2,7-bis(2-octyldodecyl) benzo[lmn][3,8]phenanthroline-1,3,6,8-tetraone monomers were synthesized according to our previously reported procedures.[22,23]

Synthesis of [Poly {[*N*, *N′*-bis(2-octyldodecyl)-naphthalene-1,4,5,8-bis(dicarboximide)-alt-5,5′-(2,2’-biselenophene)}](PNDIBS). 4,9-Dibromo-2,7-bis(2-octyldodecyl) benzo[lmn][3,8]phenanthroline-1,3,6,8-tetraone (650 mg, 0.659 mmol), 5,5’-bis(trimethylstannyl)-2,2’biselenophene (385 mg, 0.659 mmol), $Pd_2(dba)_3$ (21 mg, 3.5 mole%) and P(*o*-tolyl)$_3$ (35 mg, 0.1153 mmol) were added into a 100 mL air free Schlenk tube and then degassed and filled with argon three times. Afterwards, 30 mL chlorobenzene was added and degassed and filled with argon three times. The reaction mixture was stirred at 120 °C for 4 days under argon. The reaction mixture was cooled to 100 °C and (0.1 mL) trimethytinbenzene was added, and stirred for 12 hours followed by addition of (0.1mL) bromobenzene and stirring for another 12 hours to complete the polymer end-capping. After cooling down to room temperature, the polymerization mixture was poured into 500 mL methanol/ 10 mL hydrochloric acid solution and stirred for 3 h. The polymer precipitated out as a bluish green solid and was filtered using a buchner funnel. The polymer was purified by Soxhlet extraction sequentially with methanol, acetone, and hexane, respectively, and subsequently extracted in hot chloroform for 48h. The chloroform - insoluble fraction was removed from extraction thimble and dried in vacuum oven to give **PNDIBS (HP)** (180 mg, 26 %). The chloroform - soluble fraction was concentrated and precipitated in 400 mL methanol to give **PNDIBS (LP)** (390 mg, 55 %). **PNDIBS (LP):** ^{1}H NMR ($CDCl_3$, 500 MHz): δ (ppm) 8.85-8.50 (2H), 7.30-7.50 (4H), 4.14 (4H), 2.10 (2H), 1.40-1.15(64H), 0.80 (12H). GPC: M_w = 82.0 kDa, M_n = 28.4 kDa, $Đ$ = 2.88. TGA: T_d = 396 °C.

PNDIBS (HP): ^{1}H NMR (C_5D_5Cl, 500 MHz): δ (ppm) 8.80-8.60 (2H), 7.20-7.50 (4H), 4.14 (4H), 1.99 (2H), 1.29(64H), 0.88 (12H). GPC: M_w = 132.4 kDa, M_n = 53.7 kDa, $Đ$ = 2.46. TGA: T_d = 416 °C.

Characterizations. ^{1}H NMR spectra were recorded on a Bruker AV500 at 500 MHz using deuterated chloroform ($CDCl_3$) or chlorobenzene (C_5D_5Cl) as the solvent. Size exclusion chromatography (SEC) analysis was performed using Viscotek Gel permeation chromatography against polystyrene standards in chlorobenzene (flow rate 1mL/min) at room temperature (25 °C). GPC measurement at 120 °C was carried out by using EcoSEC high temperature system (HLC-8321GPC/HT) in 1,2,3-trichlorobenzene solvent (flow rate 1mL/min) and polystyrene standards. Thermogravimetric analysis (TGA) of the polymers was conducted on a TA Instrument model Q50TGA. A heating rate of 10 °C /min under a flow of N_2 was used with runs conducted from room temperature to 850 °C. Differential scanning calorimetry (DSC) analysis was performed on a TA Instruments Q100 under N_2 by scanning from -10 °C to 370 °C at a heating rate and cooling rate of 10 °C /min. Optical absorption spectra of polymers were measured on a PerkinElmer model Lambda 900 UV-vis/near-IR spectrophotometer. Solution and solid-state absorption spectra were obtained from dilute (10^{-6} M) polymer solution in chlorobenzene and as thin films on glass substrate, respectively. Thin films were spin-coated from 20 mg/mL solutions in chlorobenzene. Photoluminescence (PL) measurements were carried out with a Photon Technology International (PTI) Inc. model QM2001-4 spectrofluorimeter using xenon flash lamp as the light source.

Cyclic Voltammetry. Cyclic voltammetry (CV) experiments were done on an EG&G Princeton Applied Research potentiostat/galvanostat (model 273A). A three-electrode cell was used, using platinum wire electrodes as both counter and working electrode. Silver/silver ion (Ag in 0.1 M $AgNO_3$ solution) was used as a reference electrode. The films of the polymer were coated onto the

Pt wires by dipping the wires into polymer solutions in chloroform for PNDIBS (LP) and chlorobenzene for PNDIBD (HP) and then drying the coated films at 25 °C. All the CV measurements were carried out in 0.1 M tetrabutylammonium hexafluorophosphate (Bu_4NPF_6) electrolyte solution in acetonitrile at a scan rate of 50 mV/s. The reduction and oxidation potentials were referenced to the Fc/Fc^+ couple by using ferrocene as an internal standard. LUMO energy levels were estimated using ferrocene value of -4.8 eV with respect to vacuum level. The LUMO and HOMO levels were determined by using equation $E_{LUMO} = -(eE_{red}^{onset} + 4.8)$ and $E_{HOMO} = -(eE_{ox}^{onset}+4.8)$, respectively.

X-ray Diffraction (XRD) Analysis. XRD patterns were collected on a Bruker D8 Discover Microfocus diffractometer with Cu K-α beam (1.54 Å) as the X-ray source. Neat PNDIBS (LP, HP) films were prepared by drop-casting of highly concentrated solutions (20 mg/mL) in chlorobenzene onto glass substrates, and followed by annealing on a hot plate at 130 °C for 10 min. XRD patterns were recorded using $\theta/2\theta$ scans, the incident beam passed through 0.3 mm collimator and pinhole, and the incident angle between the beam and sample was fixed at 1º. The 2D-diffraction images were captured using PILATLUS3R 100-A area detector placed at 16 cm from the sample. The 1-D data (2θ vs intensity) were processed by integrating the 2-D images using EVA software.

AFM Imaging. Atomic force microscopy (AFM) characterization of the surface morphology was done on the active layers of the actual polymer solar cells, used in the photovoltaic measurements, by using a Bruker Dimension scanning probe microscope (SPM) system.

2D-GIWAXS. Grazing incidence X-ray scattering (GIWAXS) experiments were conducted at the Japan Synchrotron Radiation Facility SPring-8 by using the beamlines BL46XU and BL19B2. Thin-film samples of the neat acceptor polymers PNDIBS (LP, HP) and donor polymer PBDB-T

were respectively spin-coated on the top of glass substrates and annealed at 130 °C for 10 min and the binary blend films were prepared in the same manner as the actual all-PSC devices on ZnO-coated ITO substrates. The X-ray beam was monochromatized by a double-crystal Si (111) monochromator and the X-ray energy in this experiment was 12.40 keV (λ = 0.1 nm). The angle of incident X-ray to sample surface was 0.12º with a Huber diffractometer. The scattered profile from the film sample was detected using an area detector (PILATUS 300K) for 1 s at room temperature and the distance between the sample and detector was 174.0 mm. The crystal coherence length (L_c) of samples were analyzed by using the Scherrer equation: $Lc = 2\pi K / \Delta q$; Where K is a shape factor (typically 0.89) and Δq is the full width at half maxima (FWHM) of the diffraction peak. Here, the L_c $^{(100)}$ was obtained from the FWHM of the (100) diffraction peak in the-plane (q_{xy}) line cut.

Fabrication and characterization of Polymer Solar Cells. All-polymer solar cells were fabricated with an inverted structure of ITO/ZnO/PEI/Blend/MoO_3/Ag. ITO-coated substrates (15 Ω □$^{-1}$, Shanghai B. Tree Tech, Shanghai, China) were cleaned sequentially in ultrasonic baths with acetone and isopropyl alcohol for 15 min, dried using nitrogen gas and followed by 90 s of O_2 plasma cleaning. The ZnO precursor solution was spin-coated onto the ITO substrates at 5000 rpm for 40 s, followed by thermal annealing at 250 °C for 30 min to make ~30 nm thick ZnO layer. A 0.05 wt% solution of polyethylenimine (PEI, $M_w \approx$ 25 000, Aldrich 408727) in 2-methoxyethanol was spin-coated onto the ZnO layer and dried at 110 °C for 10 min. The solution for each PBDB-T: PNDIBS blend (1:0.4 w/w) was prepared in chlorobenzene with (or without) 0.5 vol % DPE processing additive, mixed and stirred overnight at 80 °C in the glove box. The blend solution was spin-coated at 1000 rpm for 50 s, followed by thermal annealing at 130 °C for 10 min or dried at room temperature (25 °C) for 3 h in the glove box. All the active layers had a thickness of 90 ± 10

nm. MoO_3 (0.5 nm) and Ag (100 nm) were thermally deposited onto the active layer. Each substrate contained four devices, each with an active area of 3 mm^2. After evaporation of the anode, the photovoltaic cells were tested under AM 1.5G solar illumination at 100 mW cm^{-2} in ambient air by using a solar simulator (Model 16S, Solar Light Co., Philadelphia, PA) with a 200W Xenon Lamp Power Supply (Model XPS 200, Solar Light Co., Philadelphia, PA) calibrated by NREL certified Si photodiode (Model 1787-04, Hamamatsu Photonics K.K., Japan) and a HP4155A semiconductor parameter analyzer (Yokogawa Hewlett Packard, Japan). After the *J*-*V* measurement, the external quantum efficiency (EQE) was measured by using a solar cell quantum efficiency measurement system (Model QEX10, PV Measurements, Inc., Boulder, CO) with a 2 mm (2 mm × 1 mm) size masked incident light source and TF Mini Super measurement apparatus for multiple devices in a single substrate. The EQE system was calibrated with a Si photodiode before measurement.

Space-Charge-Limited Current (SCLC) Measurement. Current-voltage (*J*-*V*) characteristics of the SCLC devices were measured by using a HP4155A semiconductor parameter analyzer (Yokogawa Hewlett-Packard, Tokyo). The carrier mobility was extracted by fitting the *J*-*V* curves according to the Mott−Gurney equation where *J* is the current density, ε_0 is the permittivity of free space, ε is the relative permittivity, μ is the zero-field mobility, *V* is the applied voltage, *d* is the thickness of active layer.

$$J = \frac{9}{8}\varepsilon\varepsilon_0\mu\frac{V^2}{d^3}$$

The SCLC device structures for hole-only and electron-only measurements were ITO/PEDOT: PSS/blends/MoO_3 (7.5 nm)/Ag (100 nm) and ITO/ZnO/PEI/blend/LiF(1 nm)/Al(100 nm), respectively. Each active layer (PBDB-T:PNDIBS (1:0.4 wt/wt)) solution in chlorobenzene with 0.5 vol% DPE processing additive was spin-coated at 1000 rpm for 50 s, followed by thermal

annealing at 130 °C for 10 min or dried at room temperature (25 °C) for 3 h (aged) in the glove box. All the active layers had thickness of 240 ± 10 nm.

2.3 RESULTS AND DISCUSSIONS

PNDIBS was synthesized by Stille coupling copolymerization of 4,9-dibromo-2,7-bis(2-octyldodecyl)-benzo[lmn][3,8]-phenanthroline-1,3,6,8-tetraone with 5,5′-Bis (trimethylstannyl)-2,2'-biselenophene in the presence of $Pd_2(dba)_3$ and P(*o*-tolyl)$_3$ in chlorobenzene following the literature procedure.[22] The PNDIBS sample was fractionated into a chloroform-soluble fraction denoted LP, which has a number-average molecular weight (M_n) of 28.4 kDa and dispersity ($Đ$) of 2.88, and a chloroform-insoluble fraction denoted HP, which has an M_n of 53.7 kDa and $Đ$ of 2.46. These M_n and Đ values also, shown in table 1 were measured at 120 °C using 1,2,3-trichlorobenzene solvent and polystyrene standards. We note that when the GPC characterization was performed at room temperature (25 °C) in chlorobenzene much higher M_n and M_w values were observed for LP (M_n = 68.8 kDa, M_w = 152 kDa) and HP (M_n = 114.6 kDa, M_w = 218 kDa), indicating significant aggregation of sample at room temperature. ^{1}H NMR spectra (Figure S1) confirmed the molecular structure of PNDIBS and were similar to prior reports.[22, 24] The LP and HP fractions had onset decomposition temperature (T_d) of 396 °C and 416 °C, respectively (Figure S2). Differential scanning calorimetry (DSC) scans (Figure S3) showed that HP had a higher melting transition temperature (T_m = 336 °C, ΔH_f = 4.79 J/g) compared to LP (T_m = 316 °C, ΔH_f = 4.20 J/g). We note that the observed M_n values for LP and HP samples are much higher compared to the previously reported M_n of 42.4 - 43.1 kDa for PNDIBS polymers with 2-decyltetradecyl[23] or 2-octyldodecyl[24] side chains. High M_n values and shorter alkyl side chains of the acceptor polymer are highly desirable for enhancing the electron mobility and face-on molecular

orientations, and for promoting intermixed domains in phase-separated nanomorphology in all-PSCs, which could all contribute to achieving higher J_{sc} and FF.[10, 29-32]

Table 1. Molecular Weight and Physical Properties of Acceptor Polymer Samples PNDIBS (LP, HP).

PNDIBS	M_n (kDa)	$Đ$	T_d (°C)	λ_{max}[a)] (nm) (log ε_{max})	λ_{max}[b)] (nm)	E_g^{opt} (eV)	d_{100} (Å)	d_{010} (Å)	fwhm	L_c (nm)
LP	68.8	2.21	396	392, 701 (4.64)	398, 722	1.40	23.70	3.90	0.57	15.4
HP	114.6	1.91	416	394, 708 (4.89)	399, 724	1.40	23.92	3.89	0.71	12.4

[a)] Absorption maximum in dilute chlorobenzene solution. [b)] Thin-film absorption maximum.

The optical absorption, electronic energy levels, and crystallinity of the neat thin films of HP and LP samples of PNDIBS were characterized to investigate any possible effects of M_n. The absorption spectra of both HP and LP showed characteristic two-bands with essentially identical peaks at 399 nm and 724 nm (Figure 2b), resulting in absorption edge optical bandgap (E_g^{opt}) of 1.40 eV. We note that the lower energy absorption band of PNDIBS, which is due to intramolecular charge transfer (ICT)[23], is redshifted from the corresponding ICT band in N2200[33] in accord with the stronger electron donating nature of biselenophene compared to the bithiophene moiety in N2200.[24, 34] Also shown in Figure 1b is the absorption spectrum of the donor polymer, PBDB-T, which nicely complements that of PNDIBS. We used onset redox potentials from cyclic voltammograms (Figure S6) to estimate the HOMO/LUMO energy levels shown in Figure 2c; no difference between HP and LP samples was observed. X-ray diffraction analysis of annealed (at 130 °C for 10 min) solution-cast films of both LP and HP revealed lamellar crystallinity with

intense (100) peaks (Figure S7). Both samples of PNDIBS also showed clear π-π stacking (010) peaks. The observed *d*-spacing values are given in the Table 1. The mean crystalline domain sizes (L_c) of the HP and LP samples calculated from the d_{100} peak using the Scherrer equation[35] were 12.4 nm and 15.4 nm, respectively, revealing effect of molecular weight.

The photovoltaic properties of all-PSCs based on PNDIBS as the acceptor component and PBDB-T as the donor component were investigated by fabricating and evaluating inverted devices with the structure: ITO/ZnO/PEI/blend/MoO_3/Ag, where polyethyleneimine (PEI) is a cathode interface layer.[36] We screened and systematically optimized the blend active layer composition and processing conditions known to determine the performance of all-PSCs, including drying of the active layer at room temperature (or aging), annealing of the active layer at a high temperature (80-175 °C), and use of various processing additives in the spin coating of the active layer from chlorobenzene solution. Representative current density-voltage (*J*-*V*) curves are collected in Figures S8-S13 and the photovoltaic parameters, including short-circuit current (J_{sc}), open circuit voltage (V_{oc}), and fill factor (FF) are provide in Tables S1-S6. We found the optimal PBDB-T:PNDIBS donor: acceptor blend composition, annealing temperature, and processing additive to be 1:0.4 wt/wt, 130 °C, and 0.5 % v/v diphenyl ether (DPE), respectively. The photovoltaic results for these optimized conditions are summarized in Figure 3 and Table 2.

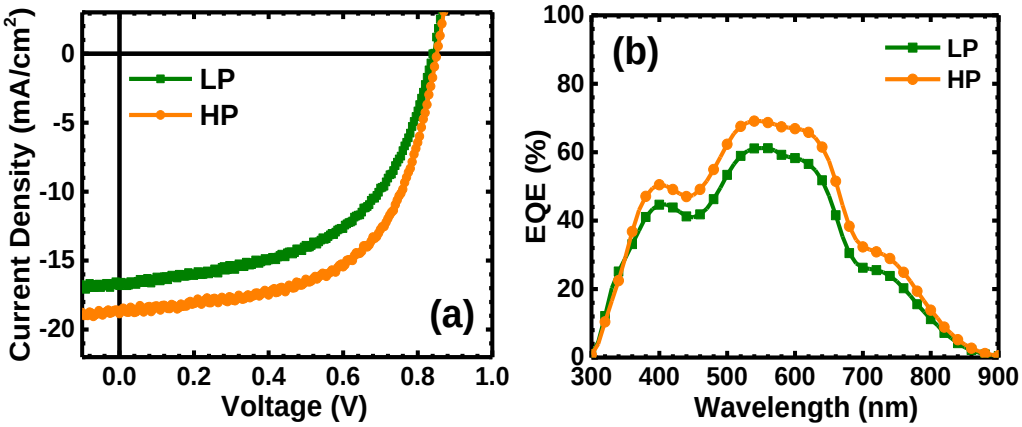

Figure 3. Current density (*J*sc)-Voltage (*V*) characteristics under AM 1.5G 100 mA/cm^2 illumination (a) and EQE spectra (b) for optimal PBDB-T:PNDIBS (LP, HP) all-polymer solar cells. The PBDB-T:LP and PBDB-T:HP blend active layers were dried at 25 °C (3 hr) and thermally annealed (130 °C,10 min), respectively.

The photovoltaic properties of the PBDB-T:LP all-PSCs, even at the optimum donor: acceptor blend composition of 1:0.4 wt/wt, varied significantly with the device processing conditions. The thermally annealed (130 °C, 10 min) devices had a PCE of 6.04% with J_{sc} of 16.1 mA/cm^2, V_{oc} of 0.83 V, and FF of 0.44. In contrast, similar devices with active layers dried in air at room temperature, had an improved PCE of 7.1% and a higher FF of 0.48 even though the J_{sc} and V_{oc} were only marginally enhanced (Table 2). This observation of enhancement of efficiency of the aged all-PSCs compared to the thermally annealed ones is very similar to a previous report for an entirely different donor/acceptor polymer pair.[6] It was suggested that the slow solvent evaporation rate during the aging at room temperature enabled the modulation of the aggregation rate of the donor and acceptor polymers and thus the nanomorphology of the all-PSC active layer.[6] The known mechanism of action of a processing additive[37, 38] is to similarly enable the differential aggregation rate of the components of an all-PSC,[39] leading to improved nanostructuring of the phase-separated morphology.[40] We thus explored four different processing additives including 1,8-

diiodooctane (DIO), 1-chloronaphthalene (CN), 1,8-octanedithiol (ODT), and diphenyl ether (DPE) and found 0.5 vol % DPE to be the best (Figure S9 and S10 and Table S2 and S3). By using DPE/chlorobenzene to fabricate PBDB-T:LP blend active layers followed by thermal annealing, we observed enhancement of FF (0.53) and the PCE, even though the J_{sc} slightly decreased (Table 2). Similar use of DPE processing additive prior to aging resulted in PBDB-T:LP all-PSC with the best performance of 7.86% PCE, which is due to the combined enhancement of J_{sc} and FF (Table 2).

Table 2. Photovoltaic Properties of 1:0.4 wt/wt PBDB-T:PNDIBS (LP, HP) Blend All-Polymer Solar Cells.

PNDIBS	Additive	Condition	J_{sc} (mA/cm^2)	V_{oc} (V)	FF	PCE_{max} (%)	PCE_{ave} (%)[c]
LP	-	Annealed[a]	16.10	0.83	0.44	6.04	5.92 (±0.22) [c]
LP	-	Aged[b]	16.16	0.85	0.48	7.12	6.63 (±0.70) [c]
LP	DPE (0.5 vol%)	Annealed[a]	15.61	0.84	0.53	6.98	6.87 (±0.10) [c]
LP	DPE (0.5 vol%)	Aged[b]	16.91	0.84	0.52	7.86	7.39 (±0.32) [d]
HP	-	Annealed[a]	18.09	0.87	0.55	8.67	8.55 (±0.12) [c]
HP	-	Aged[b]	17.42	0.87	0.52	8.02	7.89 (±0.13) [c]
HP	DPE (0.5 vol%)	Annealed[a]	18.32	0.85	0.57	9.38	8.92 (±0.29) [d]
HP	DPE (0.5 vol%)	Aged[b]	16.47	0.86	0.54	8.08	7.60 (±0.67) [c]

[a)] Annealed at 130 °C for 10 min. [b)] Aged (dried) at 25 °C for 3 hr. [c)] Average PCE values obtained from 4 separate devices. [d)] Average PCE values obtained from 15 or more separate devices.

These results clearly show that the combination of DPE processing additive and aging is synergistic in improving the performance of PBDB-T:LP all-PSCs. The performance of all-PSCs based on blends of the high-M_n PNDIBS, PBDB-T:HP, was found to be significantly enhanced compared to the above optimal PBDB-T:LP devices. Thermally annealed PBDB-T:HP devices combined enhancements of J_{sc}, FF, and even V_{oc} to achieve a PCE of 8.67% (Table 2). However, contrary to our expectations from the above low-M_n results, the aged PBDB-T:HP devices had a PCE of 8.02%, which is reduced compared to the thermally annealed cells. Interestingly, using

DPE processing additive in the solution spin coating followed by thermal annealing of the active layer, resulted in PBDB-T:HP all-PSCs with a PCE of 9.38%, J_{sc} of 18.32 mA/cm^2 and a FF of 0.57. In this case, the combination of using a DPE additive and thermal annealing has resulted in synergistic improvement of performance. However, with a PCE of 8.08%, no enhancement was observed for PBDB-T:HP cells fabricated by using DPE additive and followed by aging. This is a strikingly different result compared to the low-M_n PNDIBS devices and implies that the polymer molecular weight can dictate different pathways to optimal performance of all-PSCs.

The external quantum efficiency (EQE) spectra of the optimal PBDB-T:PNDIBS (LP, HP) devices are shown in Figure 3b. In both the low-M_n (LP) and high-M_n (HP) BHJ cells, the photoresponse and current generation turn on at 885 nm and extend to 300 nm in good agreement with the complementary absorption from the donor PBDB-T and acceptor PNDIBS polymers. Although the lineshape of the EQE spectra are similar, the HP devices have a higher EQE than the LP devices with peak EQE value of ~70% and ~60%, respectively, in the 500−650 nm region. The observed photocurrent generation in the 700-885 nm and 300-440 nm regions is largely contributed by excitons harvested by the acceptor polymer PNDIBS, suggesting that photoinduced hole transfer [26] is very efficient in this blend system. On the other hand, excitons harvested by the donor polymer PBDB-T and thus efficient photoinduced electron transfer dominate the 500−650 nm region of the EQE spectrum. We note that optical bandgap energy loss ($E_{loss} = E_g^{opt}$-eV_{oc}) in these PBDB-T:PNDIBS (LP, HP) devices is remarkably low at 0.53 eV, which is among the lowest observed so far for highly efficient all-PSCs.[12-14]

A number of the features of the observed photovoltaic properties of PBDB-T:PNDIBS devices are noteworthy for their important implications for further development of all-PSCs. First, our results demonstrate for the first time that PNDIBS is a promising electron-conducting polymer

for developing high performance all-PSCs and hence expands the scope of highly efficient acceptor polymers beyond the widely studied N2200. Second, the present findings show that a very high M_n is advantageous to improving the performance of all-PSCs and furthermore that low-M_n and high-M_n polymers can have very different pathways (e. g. aging vs thermal annealing) to the optimal performance of all-PSCs. Third, our observation of high efficiency all-PSCs from PNDIBS (LP, HP) highlights the critical roles of high M_n, suitable side chains, and choice of a donor polymer with a complementary absorption when compared to prior studies of low-M_n PNDIBS.[22, 23] Fourth, while the observed 9.4% maximum PCE for inverted PBDB-T:PNDIBS (HP) devices is among the highest so far for all-PSCs, the corresponding 57% FF value is significantly less than ~ 70-73% seen in other highly efficient all-PSC blend systems[12] and this suggests that further significant improvement in performance is possible for PNDIBS-based all-PSCs.

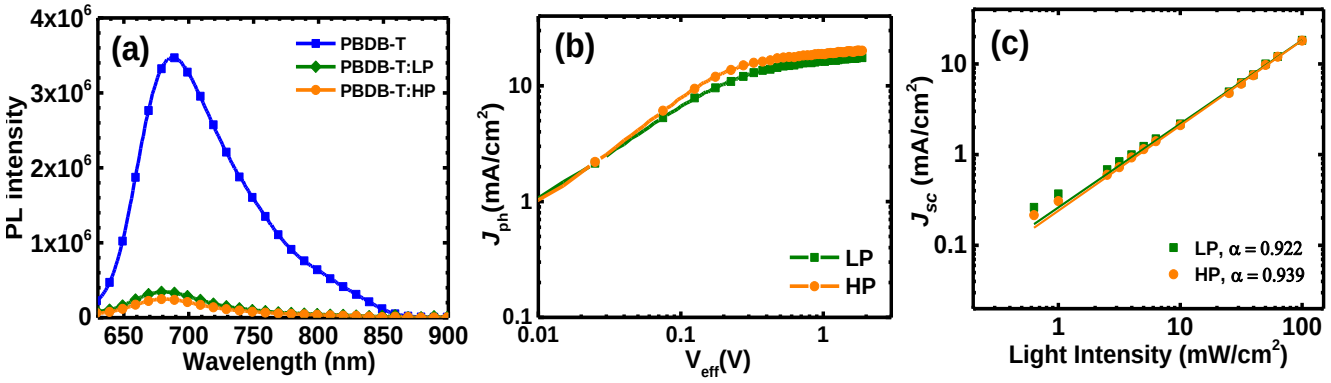

Figure 4. (a) PL emission spectra (600 nm excitation) of PBDB-T neat film and optimal PBDB-T:PNDIBS (LP, HP) blend (1:0.4 wt/wt) films. (b) J_{ph}-V_{eff} curves for optimal PBDB-T:LP and PBDB-T:HP blend devices. (c) J_{sc} dependence on light intensity for optimal PBDB-T:LP and PBDB-T:HP devices.

We performed photoluminescence (PL) quenching experiments to gain insights into exciton dissociation and charge transfer in the PBDB-T:PNDIBS (LP, HP) all-PSCs. The PL emission spectra of the optimal PBDB-T:LP and PBDB-T:HP blends (1:0.4 wt/wt) and that of the neat PBDB-T thin film are shown in Figure 4a. The broad PL emission spectrum of PBDB-T extends from 625 to 860 nm with a peak at 690 nm. Relative to this neat donor polymer emission, the PL emission spectra of the LP and HP blends are dramatically quenched with 91 and 93% quenching efficiency, respectively. These observations imply that photoinduced charge transfer is highly efficient in both the LP and HP blends. They also suggest that the nanoscale morphology of the PBDB-T:PNDIBS photovoltaic blends has sufficiently small phase-separated domains and some molecular miscibility that enabled efficient exciton dissociation.

To further understand exciton dissociation, charge photogeneration and charge collection in the PBDB-T:PNDIBS (LP, HP) blend devices, we analyzed the photocurrent density J_{ph} ($J_{ph} = J_L - J_D$) versus effective voltage V_{eff} ($V_{eff} = V_{bi} - V_a$) curves (Figure 4b), where J_L and J_D are the current densities under illumination and dark conditions, respectively, and V_{bi} is the built-in-voltage or voltage when $J_{ph} = 0$ and V_a is the applied voltage. J_{ph} is seen to slowly approach saturation at ~ 2V for both the LP and HP blend devices (Figure 4b), resulting in a saturation photocurrent density J_{sat} of 17.6 mA/cm^2 and 20 mA/cm^2, respectively. It can be concluded that the effective voltage is large enough to extract nearly all photogenerated free charges to the electrode at saturation point.[40] The maximum photoinduced carrier generation rate G_{max} can thus be estimated from the J_{sat}: ($G_{max} = J_{sat}/ q.L$), where q is the elementary charge and L is active layer thickness. For both LP and HP blend devices we obtained high G_{max} values ($\approx 10^{28}$ m^{-3} s^{-1}), which imply good exciton dissociation and charge photogeneration rates. The charge collection probability $P(E, T)$ under short circuit condition for HP devices ($= J_{ph}/J_{sat}$) was found to be 94.2%

compared to 92.4% for LP devices. The observed high G_{max} and P (E, T) values indicate that PBDB-T:PNDIBS based all-PSCs exhibit superior exciton dissociation, carrier generation, and charge collection characteristics. Furthermore, the higher P (E, T) value for HP blends suggest that the charge collection process is more efficient in the high- M_n all-PSCs.

The short-circuit current density (J_{sc}) as a function of illumination intensity (P_{light}) in the PBDB-T:PNDIBS (LP, HP) all-PSCs was measured and analyzed to understand the charge recombination kinetics of the devices. The data shown in Figure 4b follow the expected power-law dependence of J_{sc} on P_{light} ($J_{sc} \propto (P_{light})^{\alpha}$), where linearity ($\alpha = 1$) indicates weak carrier losses due to bimolecular recombination.[41] However, the observed power-law exponent α is 0.92 for LP and 0.94 for HP blend devices. We conclude that these values of α mean that there is significant carrier losses due to bimolecular recombination, which can partly explain the observed relatively low FF values (0.52−0.57) of the PBDB-T:PNDIBS all-PSCs.

We characterized the bulk charge transport of the active layers of the all-PSCs to gain further insights into the photovoltaic properties, including the FF which depends on the carrier sweep-out rate relative to bimolecular recombination rate. The bulk electron and hole mobilities of PBDB-T:PNDIBS (LP, HP) blend devices were measured by using the space charge limited current (SCLC) method with hole-only (ITO/PEDOT:PSS/active layer/MoO_3/Ag) and electron-only (ITO/ZnO/PEI/active layer/LiF/Al) structures. The J–V curves and Mott-Gurney equation fits of the data for both LP and HP blend devices are shown in Figure S13. The hole mobility (μ_h) in both LP blends (1.58×10^{-4} cm^2/Vs) and HP blends (1.93×10^{-4} cm^2/Vs) was similar and also comparable to the μ_h values reported for other BHJ devices[27] and all-PSCs[42] based on PBDB-T as the donor polymer component. In contrast, an order of magnitude higher electron mobility was observed in the HP blends ($\mu_e = 1.89 \times 10^{-4}$ cm^2/Vs) compared to the LP blends ($\mu_e = 2.33 \times 10^{-5}$

cm^2/Vs). The higher electron mobility in the high-M_n PNDIBS blends resulted in balanced charge transport (μ_h/μ_e = 1.02) in the corresponding all-PSCs in accord with the observed higher FF value (0.57) and photocurrent (J_{sc} = 18.32 mA/cm^2) compared to the more asymmetric charge transport (μ_h/μ_e = 6.78) and smaller FF (0.52) and J_{sc} (16.91 mA/cm^2) values observed in the PBDB-T:LP devices.

We investigated the surface morphology of PBDB-T:LP and PBDB-T:HP blend devices by using atomic force microscopy (AFM) imaging. AFM height and phase images of the optimal blend devices are shown in Figure S14. Both blend devices showed nearly identical phase separated morphology with domain sizes of 20-30 nm. The HP blend devices had a relatively smooth surface compared to the LP blend devices as judged by the smaller route-mean-square surface roughness value for HP blends (rms = 1.32±0.10 nm) than the LP blends (rms =1.73±0.12 nm). This observation indicates that the PBDB-T:HP blends have improved molecularly intermixed domains of the donor and acceptor polymers with suppressed macroscopic phase separation, compared to the low-M_n blends.

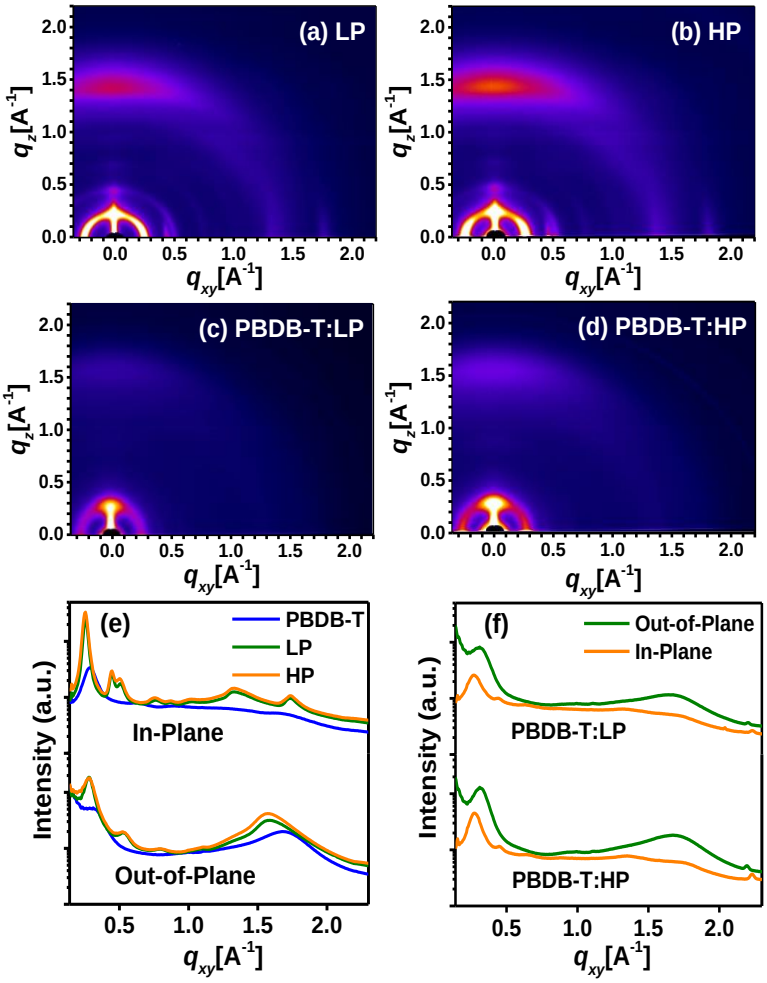

Figure 5. 2D-GIWAXS patterns of polymer thin films. (a) neat PNDIBS (LP). (b) neat PNDIBS (HP). (c, d) optimal PBDB-T:PNDIBS (LP, HP) blend (1:0.4 wt/wt) thin films: PBDB-T:LP blend dried at 25 °C for 3 h (c); PBDB-T:HP blend annealed at 130 °C for 10 min (d). (e, f) Out-of-plane and in-plane line-cut of GIWAXS patterns: neat films of LP, HP and PBDB-T thin films (e); and PBDB-T:LP and PBDB-T:HP blend thin films (f).

2D-Grazing incident wide-angle X-ray scattering (2D-GIWAXS) measurements were carried out to gain further insights into the connection of the morphology of the neat polymers and their blends to the photovoltaic properties. The 2D-GIWAXS images of the neat polymer thin films and the PBDB-T:PNDIBS (LP, HP) blend thin films are shown in Figure S14 and Figure 5,

respectively. The corresponding out-of-plane (OOP) and in-plane (IP) line cut diffractograms are also shown in Figure 5. 2D-GIWAXS pattern of neat PBDB-T film agrees with prior report:[43] OOP (010) peak for π-π stacking is observed at q_z = 1.68 Å^{-1}, and the lamellar peak (100) at q_{xy} = 0.28 Å^{-1} is located in the IP cut. Intense OOP (010) peaks (q_z = 1.58 Å^{-1}) were observed in both neat LP and HP films, indicative of adoption of face-on molecular orientation. The more intense (010) peak in the GIWAXS patterns of HP compared to LP (Figure 5) indicates that the degree of face-on molecular orientation is greater in the high-M_n PNDIBS film, similar to prior reports for other NDI-containing polymers.[29] A crystal correlation length (L_c) determined from a Scherrer equation analysis of the (100) peak for the neat PBDB-T film was found to be 5.5 nm (Table S7), which is ideal as a component to be paired with a more crystalline one in all-PSCs.[44] The similarly estimated L_c values are 16.2 nm and 15.1 nm for the LP and HP films, respectively, showing that the high-M_n PNDIBS is less crystalline although both LP and HP films are more crystalline than PBDB-T.

Our analysis of the 2D-GIWAXS results for the PBDB-T:LP and PBDB-T:HP blend films (Figure 5) revealed the following observations. First, the OOP (100) peaks are broader and shifted to larger *d*-spacing (q_z = 0.31 Å^{-1}) compared to those in the neat LP and HP films (q_z = 0.28 Å^{-1}). In both blends, the OOP (100) peak originates from PNDIBS, since the neat PBDB-T has a very weak OOP (100) peak. Similarly, the OOP (010) peak (q_z = 1.68 Å^{-1}) seen in both blends appear to originate mainly from PBDB-T. These combine features in the blend 2D-GIWAXS patterns suggest existence of some intimate mixing between the two polymers. Second, the lamellar edge-on (200) and (300) ordering peaks observed in the neat LP and HP films have disappeared in the OOP direction while weak intensity peaks are remaining in the IP direction. This suggests that crystallinity of PNDIBS is decreased in the blend films while face-on molecular orientation has significantly improved in both LP and HP blends. Third, the crystal correlation length L_c values

observed in the LP (3.7 nm) and HP (5.1 nm) blends (Table S8) found to be optimal for photovoltaic efficiency, are dramatically reduced compared to the 15-16 nm seen in the neat acceptor polymer thin films. Interestingly, the observed variation of L_c value with blend processing conditions (thermal annealing (130 °C, 10 min) versus aging (25 ^oC, 3 hr), with or without use of a DPE processing additive), clearly reveals that these processing parameters enable manipulation of the blend nanomorphology, which nicely correlates with performance of the all-PSCs. Overall, the 2D-GIWAXS results show that the nanomorphology of PBDB-T:PNDIBS blend system, including the degree of face-on molecular orientation, crystalline ordering, domain sizes, and extent of intermolecular donor/acceptor mixing, varies with the M_n of the PNDIBS sample as well as with the blend processing conditions.

2.4 CONCLUSIONS

We have synthesized high molecular weight PNDIBS and found that it can be used as an electron-conducting polymer to develop highly efficient all-PSCs. Although low-M_n PNDIBS (LP) and high-M_n PNDIBS (HP) samples have identical optical bandgap (E_g^{opt} = 1.40 eV) and HOMO/LUMO energy levels, they exhibited very different crystallinity, electron transport and photovoltaic properties. Optimal all-PSCs composed of high-M_n PNDIBS paired with donor polymer PBDB-T have a PCE of 9.4%, a J_{sc} of 18.32 mA/cm^2, and optical bandgap energy loss of 0.53 eV, which are among the best observed to date in all-PSCs. The corresponding PBDB-T:LP devices had a 7.9 % maximum PCE with a much lower photocurrent. The combined SCLC results and 2D-GIWAXS characterization of the all-PSC active layers showed that the observed large enhancement in photovoltaic properties of the high-M_n PNDIBS originates from enhanced electron mobility, greater face-on molecular orientation and more balanced charge transport. Unlike prior all-PSCs incorporating NDI-biselenophene copolymer of much lower M_n or longer side chains and

different donor polymers, which had poor efficiency (< 1%),[22,23] the present highly efficient all-PSCs thus highlight the importance of high M_n, suitable side chains, and optimal pairing with a donor polymer.

2.5 REFERENCES

(1) Halls, J. J. M.; Arias, A. C.; MacKenzie, J. D.; Wu, W.; Inbasekaran, M.; Woo, E. P.; Friend, R. H. *Adv. Mater.* **2000,** *12*, 498-502.

(2) Jenekhe, S. A.; Yi, S. *Appl.Phys. Lett.* **2000,** *77*, 2635-2637.

(3) Facchetti, A. *Mater. Today* **2013,** *16*, 123-132.

(4) Benten, H.; Mori, D.; Ohkita, H.; Ito, S. *J. Mater. Chem. A* **2016,** *4*, 5340-5365.

(5) Kang, H.; Lee, W.; Oh, J.; Kim, T.; Lee, C.; Kim, B. J. *Acc. Chem. Res.* **2016,** *49*, 2424-2434.

(6) Hwang, Y.-J.; Courtright, B. A. E.; Ferreira, A. S.; Tolbert, S. H.; Jenekhe, S. A. *Adv. Mater.* **2015,** *27*, 4578-4584.

(7) Lu, L.; Zheng, T.; Wu, Q.; Schneider, A. M.; Zhao, D.; Yu, L. *Chem. Rev.* **2015,** *115*, 12666-12731.

(8) Kim, T.; Kim, J.-H.; Kang, T. E.; Lee, C.; Kang, H.; Shin, M.; Wang, C.; Ma, B.; Jeong, U.; Kim, T.-S.; Kim, B. J. *Nat. Commun.* **2015,** *6*, 8547.

(9) Lin, Y.; Dong, S.; Li, Z.; Zheng, W.; Yang, J.; Liu, A.; Cai, W.; Liu, F.; Jiang, Y.; Russell, T. P.; Huang, F.; Wang, E.; Hou, L. *Nano Energy* **2018,** *46*, 428-435.

(10) Earmme, T.; Hwang, Y.-J.; Murari, N. M.; Subramaniyan, S.; Jenekhe, S. A. *J. Am. Chem. Soc.* **2013,** *135*, 14960-14963.

(11) Gao, L.; Zhang, Z.-G.; Xue, L.; Min, J.; Zhang, J.; Wei, Z.; Li, Y. *Adv. Mater.* **2016,** *28*, 1884-1890.

(12) Fan, B.; Ying, L.; Zhu, P.; Pan, F.; Liu, F.; Chen, J.; Huang, F.; Cao, Y. *Adv. Mater.* **2017,** *29*, 1703906.

(13) Fan, B.; Ying, L.; Wang, Z.; He, B.; Jiang, X.-F.; Huang, F.; Cao, Y. *Energy & Environ Sci.* **2017,** *10*, 1243-1251.

(14) Li, Z.; Xu, X.; Zhang, W.; Meng, X.; Genene, Z.; Ma, W.; Mammo, W.; Yartsev, A.; Andersson, M. R.; Janssen, R. A. J.; Wang, E. *Energy & Environ Sci.* **2017,** *10*, 2212-2221.

(15) Guo, Y.; Li, Y.; Awartani, O.; Han, H.; Zhao, J.; Ade, H.; Yan, H.; Zhao, D. *Adv. Mater.* **2017,** *29*, 1700309.

(16) Zhao, J.; Li, Y.; Yang, G.; Jiang, K.; Lin, H.; Ade, H.; Ma, W.; Yan, H. *Nat. Energy* **2016,** *1*, 15027.

(17) Wan, Q.; Guo, X.; Wang, Z.; Li, W.; Guo, B.; Ma, W.; Zhang, M.; Li, Y. *Adv. Funct. Mater.* **2016,** *26*, 6635-6640.

(18) Jin, Y.; Chen, Z.; Dong, S.; Zheng, N.; Ying, L.; Jiang, X.-F.; Liu, F.; Huang, F.; Cao, Y. *Adv. Mater.* **2016,** *28*, 9811-9818.

(19) Janssen, R. A. J.; Nelson, J. *Adv. Mater.* **2013,** *25*, 1847-1858.

(20) Giebink, N. C.; Wiederrecht, G. P.; Wasielewski, M. R.; Forrest, S. R. *Phys. Rev. B* **2011,** *83*, 195326.

(21) Hwang, Y.-J.; Murari, N. M.; Jenekhe, S. A. *Polym. Chem.* **2013,** *4*, 3187-3195.

(22) Hwang, Y.-J.; Ren, G.; Murari, N. M.; Jenekhe, S. A. *Macromolecules* **2012,** *45*, 9056-9062.

(23) Shi, S.; Yuan, J.; Ding, G.; Ford, M.; Lu, K.; Shi, G.; Sun, J.; Ling, X.; Li, Y.; Ma, W. *Adv. Funct. Mater.* **2016,** *26*, 5669-5678.

(24) Li, S.; Ye, L.; Zhao, W.; Zhang, S.; Mukherjee, S.; Ade, H.; Hou, J. *Adv. Mater.* **2016,** *28*, 9423-9429.

(25) Ye, L.; Jiao, X.; Zhao, W.; Zhang, S.; Yao, H.; Li, S.; Ade, H.; Hou, J. *Chem. Mater.* **2016,** *28*, 6178-6185.

(26) Ren, G.; Schlenker, C. W.; Ahmed, E.; Subramaniyan, S.; Olthof, S.; Kahn, A.; Ginger, D. S.; Jenekhe, S. A. *Adv. Funct. Mater.* **2013,** *23*, 1238-1249.

(27) Zhang, Z.-G.; Yang, Y.; Yao, J.; Xue, L.; Chen, S.; Li, X.; Morrison, W.; Yang, C.; Li, Y. *Angew. Chem. Int. Ed.* **2017,** *56*, 13503-13507.

(28) Lee, W.; Lee, C.; Yu, H.; Kim, D.-J.; Wang, C.; Woo, H. Y.; Oh, J. H.; Kim, B. J. *Adv. Funct. Mater.* **2016,** *26*, 1543-1553.

(29) Jung, J.; Lee, W.; Lee, C.; Ahn, H.; Kim, B. J. *Adv. Energy Mater.* **2016,** *6*, 1600504.

(30) Zhou, N.; Dudnik, A. S.; Li, T. I. N. G.; Manley, E. F.; Aldrich, T. J.; Guo, P.; Liao, H.-C.; Chen, Z.; Chen, L. X.; Chang, R. P. H.; Facchetti, A.; Olvera de la Cruz, M.; Marks, T. J. *J. Am. Chem. Soc.* **2016,** *138*, 1240-1251.

(31) Chen, S.; An, Y.; Dutta, G. K.; Kim, Y.; Zhang, Z.-G.; Li, Y.; Yang, C. *Adv. Funct. Mater.* **2017,** *27*, 1603564.

(32) Chen, Z.; Zheng, Y.; Yan, H.; Facchetti, A. *J. Am. Chem. Soc.* **2009,** *131*, 8-9.

(33) Ashraf, R. S.; Meager, I.; Nikolka, M.; Kirkus, M.; Planells, M.; Schroeder, B. C.; Holliday, S.; Hurhangee, M.; Nielsen, C. B.; Sirringhaus, H.; McCulloch, I. *J. Am. Chem. Soc.* **2015,** *137*, 1314-1321.

(34) Patterson, A. L., The Scherrer Formula for X-Ray Particle Size Determination. *Phy. Rev.* **1939,** *56*, 978-982.

(35) Courtright, B. A. E.; Jenekhe, S. A. *ACS Appl. Mater. Interfaces* **2015,** *7*, 26167-26175.

(36) Lee, J. K.; Ma, W. L.; Brabec, C. J.; Yuen, J.; Moon, J. S.; Kim, J. Y.; Lee, K.; Bazan, G. C.; Heeger, A. J. *J. Am. Chem. Soc.* **2008,** *130*, 3619-3623.

(37) Xin, H.; Guo, X.; Kim, F. S.; Ren, G.; Watson, M. D.; Jenekhe, S. A. *J. Mater. Chem.* **2009,** *19*, 5303-5310.

(38) Shi, G.; Yuan, J.; Huang, X.; Lu, Y.; Liu, Z.; Peng, J.; Ding, G.; Shi, S.; Sun, J.; Lu, K.; Wang, H.-Q.; Ma, W. *J. Phys. Chem. C* **2015,** *119*, 25298-25306.

(39) Yuan, J.; Ma, W. *J. Mater. Chem. A* **2015,** *3*, 7077-7085.

(40) Mori, D.; Benten, H.; Okada, I.; Ohkita, H.; Ito, S. *Energy & Environ Sci.* **2014,** *7*, 2939-2943.

(41) Schilinsky, P.; Waldauf, C.; Brabec, C. J. *Appl.Phys. Lett.* **2002,** *81*, 3885-3887.

(42) Zhao, W.; Qian, D.; Zhang, S.; Li, S.; Inganäs, O.; Gao, F.; Hou, J. *Adv. Mater.* **2016,** *28*, 4734-4739.

(43) Xu, S. j.; Zhou, Z.; Liu, W.; Zhang, Z.; Liu, F.; Yan, H.; Zhu, X. *Adv. Mater.* **2017,** *29*, 1704510.

(44) Hwang, Y.-J.; Earmme, T.; Courtright, B. A. E.; Eberle, F. N.; Jenekhe, S. A. *J. Am. Chem. Soc.* **2015,** *137*, 4424-4434

Chapter 3. ALL-POLYMER SOLAR CELLS BASED ON RANDOM COPOLYMER ACCEPTORS

3.1 INTRODUCTION

Photoactive layer of all-polymer solar cells (all-PSCs) contains two class of semiconducting polymers, one with electron-conducting (acceptor) and other with hole-conducting (donor) behavior.[1-7] They have attracted much attention in recent years due to their tremendous potential over polymer/fullerene composite solar cells. Electron-conducting polymer used in all-PSCs as a replacement for fullerene derivative has many unique features like low-cost, high thermal/photochemical stability, enhanced light-harvesting properties, a good tunability of molecular and electronic structure, and mechanical robustness and flexibility; therefore, increasing its feasibility for scaling up on the larger scale in an inexpensive way.[6, 8, 9] In addition to the aforementioned promising features, the performance of all-PSCs regarding power conversion efficiency (PCE) has been rapidly increased from 2% to about 8-10% over the past five years, [6, 10-15] indicating the great promise of the all-PSCs based technology for future real-world applications. Nonetheless, the device performance of state-of-the-art all-PSCs still lag behind the fullerene and other emerging small-molecule acceptor-based PSCs[16-19]; a very few of the all-PSCs exhibited PCEs over 8%.[11-14] In general, the inferior device performance of all-PSCs is often correlated to the suboptimal bulk-heterojunction (BHJ) morphology of polymer:polymer blend that resulted in the unfavorable conditions for efficient exciton generation and/or charges transport. Such suboptimal morphology could be identified by the commonly observed low fill factor (FF) and low photocurrent (J_{sc}) values. Therefore, although it is a challenging task,[20, 21] controlling the

polymer:polymer blend film morphology is highly desirable to enhance the device parameters (FF and J_{sc}) of all-PSCs.

Thin film morphology of all-PSC is highly dependent on the nature of photoactive (or semiconducting) polymers: their molecular structure, side chain, and molecular weight.[10, 13, 20, 22-24] Considering these factors, a lot of efforts have been devoted in the past two decades to develop new semiconducting polymers, both electron-donor and electron-acceptor that helped to improve the blend morphology and overall PCE of all-PSCs.[3, 4, 7] Among these photoactive materials, the polymers developed by using random copolymer design approach, utilizing three different types of monomers in the single backbone have been more appealing to tune the morphological and optoelectronic properties of relevant polymers.[25] In this regard, our group has demonstrated that the bulk crystallinity of naphthalene diimide (NDI)-selenophene/perylene diimide (PDI)-selenophene *n*-type random copolymers can be well tuned by varying the composition of NDI and PDI monomers in backbone.[26] We found that the bulk crystallinity of polymer is a critical factor in determining the compatibility and blend morphology of all-PSCs. Random copolymer design strategy adopted in our study was found to be an easy, robust and reliable method to achieve an optimum all-PSC blend morphology, resulting in the large enhancement in the photovoltaic efficiency of all-PSC. By implementing this strategy, several naphthalene-diimide (NDI) and perylene-diimide (PDI) based acceptor random copolymers were synthesized by others[27-32], which were reported to greatly enhance the device efficiency as compared to their reference homo-polymers. Indeed, even in case of appealing acceptor polymer NDI-bithiophene (N2200), its random copolymer acceptors [29, 33, 34] showed improved all-PSC device efficiency as compared to N2200 homo-polymer.

It is very rare to achieve the optimum thin film morphology by using the above-mentioned chemical approaches alone, rather in common practice the desired morphology was achieved by using external post-processing treatments such as thermal annealing, solvent annealing, solvent aging, co-solvent, and solvent additives.[6, 12, 33, 35-38] Even the random copolymer acceptor-based high performing all-PSC reported so far utilizes solvent additives to realize the optimum morphology.[26, 33, 34] However, these techniques are not only making device complexity and fabrication process more challenging but also create the issue of device stability.[39, 40] In general, the thermal annealing of donor and acceptor polymer beyond the glass transition temperature is helpful to improve the thin film morphology and device efficiency of all-PSCs. However, the rigid and planar structure of most of the acceptor polymer leads to the large domain sizes and phase separation under thermal annealing, resulting in the improper donor/acceptor mixing and poor thin film morphology.[41] Therefore, it is necessary to develop a new polymer acceptor with controlled bulk crystallinity, molecular ordering while improving the thermal stability without the use of solvent additive and tedious processing treatments to achieve a high-performance stable and scalable all-PSCs.

In this Chapter, I reported the synthesis and characterization of a novel series of random copolymers (BSS*x*) and utilized them as an electron accepting component in all-PSCs. The molecular structure of random copolymers (BSS*x*) (Figure 6a) is a combination of NDI-biselenophene/NDI-selenophene backbone in which a certain amount of electron-donating biselenophene (BS) units of BSS0 are replaced by selenophene (S*x*), where *x* represents the percentage of selenophene. The molar percentage incorporation of selenophene was 10% 20%, and 50%, leading to the polymers BSS10, BSS20, and BSS50 respectively. The consequence of different composition of (BS) versus (S) on the random copolymer behavior was characterized

systematically by analyzing thermal, photophysical, morphological, and charge transport properties. We found that the crystallinity and molecular orientation of random copolymers were significantly changed as compared to BSS0 reference sample. As a result, they form a compatible blend with PBDB-T donor polymer with favorable morphology, higher electron mobilities, and symmetric charge transport. BSS20-based all-PSC exhibited an enhanced photovoltaic parameter with maximum PCE of 9.6% and J_{sc} of 19.70 mA/cm^2. This PCE value is among the highest reported so far for all-PSCs by employing random copolymer as an electron acceptor component. Interestingly, unlike other literature reported random copolymer-based all-PSCs,[26, 29, 33, 34] thin film morphology optimization in these random copolymer -based all-PSCs had been achieved without using any solvent additives or/and tedious post-processing treatment. Moreover, the all-PSCs device morphology is thermally stable up to 200 °C.

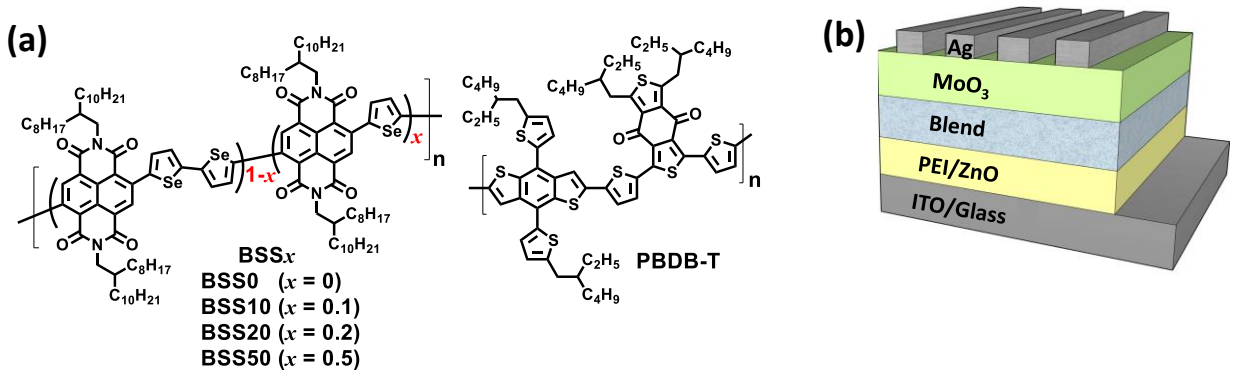

Figure 6. (a) Molecular structures of the acceptor (BSS*x*) and donor (PBDB-T) copolymers. (b) Schematic of the inverted all-PSC device.

3.2 Experiment Section

Materials. Tri-(*o*-tolyl)-phosphine, tris(dibenzylideneacetone)dipalladium (0) ($Pd_2(dba)_3$), selenophene, trimethyltin chloride (20% solution) in THF, anhydrous copper(II)chloride, *n*-butyl lithium (2M in hexane), and chlorobenzene were purchased from Sigma-Aldrich and used without

further purification. 5,10-Dibromoisochromeno[6,5,4-*def*] isochromene-1,3,6,8(*3aH, 8aH*)-tetraone and 2-octyldodecyl amine were purchased from Suna Tech Inc (Jaiansu, China). The donor polymer PBDB-T (M_n = 62 kDa, $Đ$ = 1.90) was purchased from Brilliant Matters Organic electronics (Quebec, Canada) and was used as received.

Synthesis.

Monomer Synthesis. 5,5′-bis (trimethylstannyl)-2,2'-biselenophene, 2,5-bis (trimethylstannyl)-selenophene and 4,9-dibromo-2,7-bis(2-octyldodecyl) benzo[lmn][3,8]phenanthroline-1,3,6,8-tetraone monomers were synthesized according to our previously reported procedures.

Synthesis of [Poly {[*N,N′*-bis(2-octyldodecyl)-naphthalene-1,4,5,8-bis(dicarboximide)-2,6-diyl]-*alt*-5,5′-(2,2'-biselenophene)}-*ran*-{[*N,N′*-bis(2-octyldodecyl)-naphthalene-1,4,5,8 bis(dicarboximide)-2,6-diyl]-*alt*-5,5′-(selenophene)] (BSS*x*).

Copolymer BSS10

4,9-Dibromo-2,7-bis(2-octyldodecyl) benzo[lmn] [3,8] phenanthroline-1,3,6,8-tetraone (550 mg, 0.558 mmol), 5,5'-bis(trimethylstannyl)-2,2'biselenophene (294 mg, 0.502 mmol), 2,5-bis (trimethylstannyl)-selenophene (26 mg, 0.055 mmol), $Pd_2(dba)_3$ (20 mg, 3.5 mole%) and P(*o*-tolyl)$_3$ (32.5 mg) were added into a 100-mL air free Schlenk tube and then degassed and filled with argon three times. Afterwards, 25 mL chlorobenzene was added and degassed and filled with argon three times. The reaction mixture was stirred at 120 °C for 4 days under argon. The reaction mixture was cooled to 100 °C and (0.1 mL) trimethytinbenzene was added and stirred for 12 hours followed by addition of (0.1mL) bromobenzene and stirring for another 12 hours to complete the polymer end-capping. After cooling down to room temperature, the polymerization mixture was poured into 500 mL methanol/ 10 mL hydrochloric acid solution and stirred for 3 h. The polymer precipitated out as a bluish green solid and was filtered using a buchner funnel. The polymer was

purified by Soxhlet extraction sequentially with methanol, acetone, and hexane, respectively, and subsequently extracted in hot chloroform for 3h. The chloroform was concentrated and precipitated in 400 mL methanol to give **BSS10** (Yield, 560 mg, 93 %).

Copolymer BSS20

It was synthesized by using similar procedure as mentioned above, starting with 4,9-Dibromo-2,7-bis(2-octyldodecyl) benzo[lmn] [3,8] phenanthroline-1,3,6,8-tetraone (500 mg, 0.507 mmol), 5,5'-bis(trimethylstannyl)-2,2'biselenophene (237 mg, 0.406 mmol), 2,5-bis (trimethylstannyl)-selenophene (47 mg, 0.101mmol), $Pd_2(dba)_3$ (20 mg, 3.5 mole%) and P(*o*-tolyl)$_3$ (32.5 mg). Yield, 520 mg, 95%).

Copolymer BSS50

It was synthesized by using similar procedure as mentioned above, starting with 4,9-Dibromo-2,7-bis(2-octyldodecyl) benzo[lmn] [3,8] phenanthroline-1,3,6,8-tetraone (500 mg, 0.507 mmol), 5,5'-bis(trimethylstannyl)-2,2'biselenophene (148 mg, 0.253 mmol), 2,5-bis (trimethylstannyl)-selenophene (115 mg, 0.0.253mmol), $Pd_2(dba)_3$ (20 mg, 3.5 mole%) and P(*o*-tolyl)$_3$ (32.5 mg). Yield, 450 mg, 75%).

Characterizations. ^{1}H NMR spectra were recorded on a Bruker AV500 at 500 MHz using deuterated chloroform ($CDCl_3$) as the solvent at 329 K. Size exclusion chromatography (SEC) analysis was performed using EcoSEC High temperature GPC system (HLC-8321GPC/HT) against polystyrene standards in chlorobenzene 1,2,3-trichlorobenzene at 120 °C (flow rate 1mL/min). Thermogravimetric analysis (TGA) of the polymers was conducted on a TA Instrument model Q50TGA. A heating rate of 10 °C /min under a flow of N_2 was used with runs conducted from room temperature to 850 °C. Differential scanning calorimetry (DSC) analysis was performed on a TA Instruments Q100 under N_2 by scanning from -10 °C to 370 °C at a heating

rate and cooling rate of 10 °C /min. Optical absorption spectra of polymers were measured on a PerkinElmer model Lambda 900 UV-vis/near-IR spectrophotometer. Solution and solid-state absorption spectra were obtained from dilute (10^{-6} M) polymer solution in chloroform and as thin films on glass substrate, respectively. Thin films were spin coated from 20 mg/mL solutions in chlorobenzene. Photoluminescence (PL) measurements were carried out with a Photon Technology International (PTI) Inc. model QM2001-4 spectrofluorimeter using xenon flash lamp as the light source.

Cyclic Voltammetry. Cyclic voltammetry (CV) experiments were done on an EG&G Princeton Applied Research potentiostat/galvanostat (model 273A). A three-electrode cell was used, using platinum wire electrodes as both counter and working electrode. Silver/silver ion (Ag in 0.1 M $AgNO_3$ solution) was used as a reference electrode. The films of the random copolymer were coated onto the Pt wires by dipping the wires into copolymer solutions in chloroform for then drying the coated films at 25 °C. All the CV measurements were carried out in 0.1 M tetrabutylammonium hexafluorophosphate (Bu_4NPF_6) electrolyte solution in acetonitrile at a scan rate of 50 mV/s. The reduction and oxidation potentials were referenced to the Fc/Fc^+ couple by using ferrocene as an internal standard. LUMO energy levels were estimated using ferrocene value of -4.8 eV with respect to the vacuum level. The LUMO and HOMO levels were determined by using equation[30] $E_{LUMO} = -(eE_{red}^{onset} + 4.8)$ and $E_{HOMO} = -(eE_{ox}^{onset}+4.8)$, respectively.

X-ray Diffraction (XRD) Analysis. XRD patterns were collected on a Bruker D8 Discover Microfocus diffractometer with Cu K-α beam (1.54 Å) as the X-ray source. Neat films of random copolymers and reference PNDIBS were prepared by drop-casting of highly concentrated solutions (20 mg/mL) in chlorobenzene onto glass substrates and followed by annealing on a hot plate at 130 °C for 10 min. XRD patterns were recorded using $\theta/2\theta$ scans, the incident beam passed through

0.3 mm collimator and pinhole, and the incident angle between the beam and sample was fixed at 1º. The 2D-diffraction images were captured using PILATLUS3R 100-A area detector placed at 16 cm from the sample. The 1-D data (2θ vs. intensity) were processed by integrating the 2-D images using EVA software.

AFM Imaging. Atomic force microscopy (AFM) characterization of the surface morphology was done on the active layers of the actual polymer solar cells, used in the photovoltaic measurements, by using a Bruker Dimension scanning probe microscope (SPM) system.

2D-GIWAXS.

Grazing incidence X-ray scattering (GIWAXS) experiments were conducted at the Japan Synchrotron Radiation Facility SPring-8 by using the beamlines BL46XU and BL19B2. Thin-film samples of the neat acceptor polymers (BSS*x*) and donor polymer PBDB-T were respectively spin-coated on the top of glass substrates and annealed at 175 °C for 10 min, and the binary blend films were prepared in the same manner as the actual all-PSC devices on ZnO-coated ITO substrates. The X-ray beam was monochromatized by a double-crystal Si (111) monochromator and the X-ray energy in this experiment was 12.40 keV (λ = 0.1 nm). The angle of incident X-ray to sample surface was 0.12º with a Huber diffractometer. The scattered profile from the film sample was detected using an area detector (PILATUS 300K) for 1 s at room temperature, and the distance between the sample and detector was 174.0 mm. The crystal coherence length (L_c) of samples were analyzed by using the Scherrer equation: $Lc = 2\pi K / \Delta q$; Where K is a shape factor (typically 0.89) and Δq is the full width at half maxima (FWHM) of the diffraction peak. Here, the L_c $^{(100)}$ was obtained from the FWHM of the (100) diffraction peak in the-plane (q_{xy}) line cut.

Fabrication and characterization of Polymer Solar Cells.

All-polymer solar cells were fabricated with an inverted structure of ITO/ZnO/PEI/Blend/MoO_3/Ag. ITO-coated substrates (15 Ω □$^{-1}$, Shanghai B. Tree Tech, Shanghai, China) were cleaned sequentially in ultrasonic baths with acetone and isopropyl alcohol for 15 min, dried using nitrogen gas and followed by 90 s of O_2 plasma cleaning. The ZnO precursor solution was spin-coated onto the ITO substrates at 5000 rpm for 40 s, followed by thermal annealing at 250 °C for 30 min to make ~30 nm thick ZnO layer. A 0.05 wt% solution of polyethylenimine (PEI, $M_w \approx 25\,000$, Aldrich 408727) in 2-methoxyethanol was spin-coated onto the ZnO layer and dried at 110 °C for 10 min. The solution for each PBDB-T:BSS*x* blend (1:0.6 w/w) was prepared in chlorobenzene, mixed and stirred overnight at 80 °C in the glove box. The blend solution was spin-coated at 1000 rpm for 50 s, followed by thermal annealing at 175 °C for 10 min in the glove box. All the active layers had a thickness of 100 ± 10 nm. MoO_3 (0.5 nm) and Ag (100 nm) were thermally deposited onto the active layer. Each substrate contained four devices, each with an active area of 3 mm^2. After evaporation of the anode, the photovoltaic cells were tested under AM 1.5G solar illumination at 100 mW cm^{-2} in ambient air by using a solar simulator (Model 16S, Solar Light Co., Philadelphia, PA) with a 200W Xenon Lamp Power Supply (Model XPS 200, Solar Light Co., Philadelphia, PA) calibrated by NREL certified Si photodiode (Model 1787-04, Hamamatsu Photonics K.K., Japan) and a HP4155A semiconductor parameter analyzer (Yokogawa Hewlett Packard, Japan). After the *J-V* measurement, the external quantum efficiency (EQE) was measured by using a solar cell quantum efficiency measurement system (Model QEX10, PV Measurements, Inc., Boulder, CO) with a 2 mm (2 mm × 1 mm) size masked incident light source and TF Mini Super measurement apparatus for multiple devices in a single substrate. The EQE system was calibrated with a Si photodiode before measurement.

SCLC Device Fabrication

Current-voltage (*J*-*V*) characteristics of the SCLC devices were measured by using a HP4155A semiconductor parameter analyzer (Yokogawa Hewlett-Packard, Tokyo). The carrier mobility was deduced by fitting the *J*-*V* curves to the Mott−Gurney equation where *J* is the current density, ε_0 is the permittivity of free space, ε is the relative permittivity, μ is the zero-field mobility, *V* is the applied voltage, *d* is the thickness of the active layer. $J = \frac{9}{8}\varepsilon\varepsilon_0\mu\frac{V^2}{d^3}$ The SCLC device structures for electron only and hole only were ITO/ZnO/PEI/blend/LiF (2nm)/Al (100nm) and ITO/PEDOT:PSS/blends/MoO_3 (7.5nm)/Ag (100nm), respectively. Each active layer, which was comprised of chlorobenzene solutions of PBDB-T and acceptor polymers (BSS*x*) at D/A ratio of 1 to 0.6, was spin-coated at 1000 rpm for 50s and followed by thermal annealing at 175^{o}C for 10 min inside the glovebox. All active layers had a thickness of 175 ± 10 nm.

3.3 Results and Discussions

A novel series of electron deficient (*n*-type) random copolymers (BSS*x*) were synthesized by Stille coupling polymerization of electron-accepting 4,9-dibromo-2,7-bis(2-octyldodecyl)-benzo[lmn] [3,8]-phenanthroline-1,3,6,8-tetraone with two electron-donating monomers, 5,5'-bis(trimethylstannyl)-2,2'selenophene and 2,5-bis(trimethylstannyl)-selenophene. The required monomers for polymerization were synthesized and purified by following our previously reported procedures.[20, 24, 40] Random copolymers showed excellent solubility in common organic solvents, including chloroform, chlorobenzene, and dichlorobenzene at room temperature. The molecular structure of the copolymer was confirmed by ^{1}H NMR spectra (Figure S1a, b, and c), all the spectra were recorded in $CDCl_3$ (5-6 mg/mL) at 329 K. Similar to ^{1}H NMR spectra reported for BSS0 polymer in our previous work,[40] copolymer BSS10 shows peak at 8.87-8.57 ppm for NDI (Figure S1a) and 7.40-7.52 ppm for biselenophene aromatic protons, while there is no detectable separate

peak was observed for NDI/selenophene backbone. In contrast, the copolymer BSS20 and BSS50 which has higher incorporation of selenophene unit, shows separate peaks for NDI/selenophene backbone (NDI at ~ 9.00 ppm and selenophene at ~7.65 ppm) in addition to the peaks for NDI-biselenophene, confirming the incorporation selenophene in random copolymer backbone.

Table 3. Molecular Weight, Optical Properties, and Decomposition Temperature of BSS*x* copolymers.

Polymer	M_n (kDa)	$Đ$	λ_{max} (nm) [a] ($\log \varepsilon$ $M^{-1}cm^{-1}$)	λ_{max} (nm)[b]	E_g^{opt} (eV)	T_d (℃)	ΔH_m (J/g)
BSS0	28.4	2.88	392, 695 (4.36)	393, 720	1.40	396	4.20
BSS10	41.7	2.82	388, 675 (4.41)	393, 703	1.45	406	2.31
BSS20	33.2	2.54	386, 659 (4.28)	392, 698	1.46	386	-
BSS50	-	-	384, 615 (4.14)	387, 668	1.50	388	1.26

[a)] Absorption maximum in dilute chloroform solution. [b)] Thin-film absorption maximum.

The molecular weight and polydispersity index ($Đ$) of the BSS*x* copolymers were measured by gel permeation chromatography (GPC) in 1,2,3-trichlorobenzene solvent at 120 °C using polystyrene as standards. As depicted in Table3, BSS*x* copolymers had a number-average molecular weight (M_n) in the range of 28.4-41.7 kDa with a polydispersity ($Đ$) of 2.54-2.88. It is to be noted that BSS0 reference sample utilized in the present study was previously synthesized in our lab and had M_n (28.4 kDa) and $Đ$ (2.88). The slightly higher M_n of random copolymers was attributed to the improved solubility. Overall, the incorporation of selenophene has a small effect on the molecular weights of resulting polymers; therefore, it is worth to use BSS0 sample to compare with the all-PSCs performance of new random copolymers.

Thermogravimetric analysis (TGA) of BSS*x* copolymers showed good thermal stability with onset decomposition temperature (T_d) of over 385 °C (Table 3) under nitrogen flow (Figure

S2). Differential scanning colorimetry (DSC) analysis was carried out to determine the thermal transitions and crystalline/amorphous nature of random copolymers. The second heating and cooling curves of BSS*x* copolymers are shown in Figure S3. The BSS0, BSS10, and BSS50 random copolymer showed a significantly broad melting transition (T_m) during heating and crystallization transition (T_c) during the cooling cycle. Meanwhile, both the T_m and T_c of BSS20 were not detectable by DSC. The BSS0 showed higher T_m (316 °C) than the BSS10 (T_m = 298 °C) and BSS50 (T_m = 235 °C) which evinces that the incorporation of selenophene unit resulted in the reduced planarity or/rigidity and chain stacking in the random copolymer. Also, BSS10 and BSS50 showed lower melting enthalpy ΔH_m (2.31 J/g) and ΔH_m (1.26 J/g), respectively as compared to BSS0 (ΔH_m = 4.20 J/g) indicating that the crystallinity of random copolymers is reduced due to increased backbone disorder. Overall, the thermal properties confirm the more flexible and less crystalline nature of the random copolymers as compared to reference BSS0 which is highly desirable to achieve a miscible blend with donor polymers; thereby the suitable nanoscale phase separated D/A morphology in all-PSCs.[24, 31]

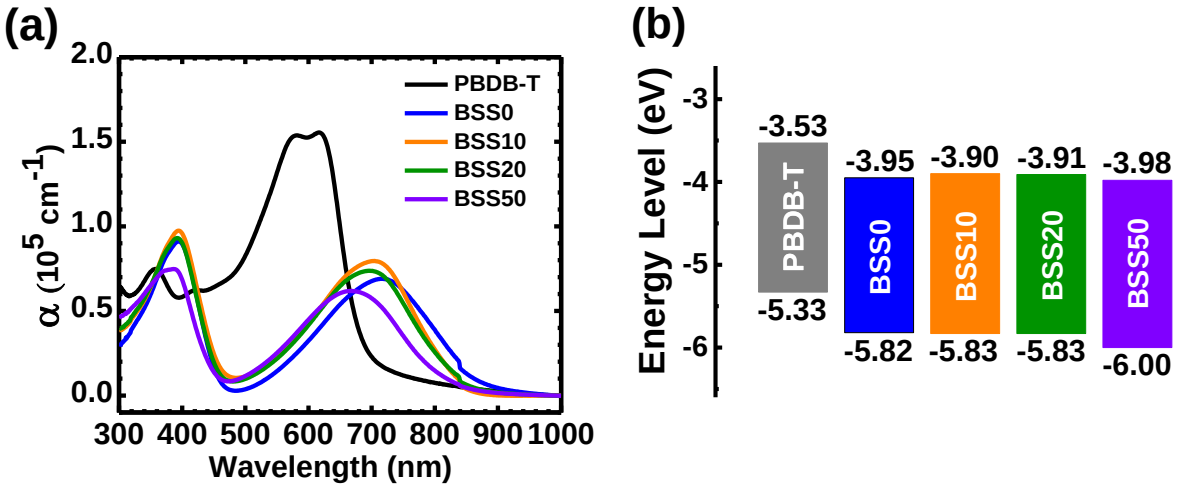

Figure 7. Thin film optical absorption spectra (a) and HOMO/LUMO energy levels (b) of donor and acceptor copolymers.

The optical absorption properties of new random copolymers were characterized by UV-vis-near IR absorption spectroscopy of dilute (10^{-5} M) chloroform solution (FigureS4) and thin films on a glass substrate (Figure 7a). The spectra for reference BSS0 was also recorded at similar conditions. Similar to reported for other well-known NDI polymers[10, 20] the chloroform solution of BSS*x* copolymers showed two distinct absorption bands at 300-450 nm and 500-850 nm, which was assigned to π-π* or n-π* transition of NDI moiety and an intramolecular charge transfer (ICT) band, respectively. Reference sample BSS0 showed absorption maxima at 392 nm and 695 nm. After introducing the selenophene moiety, the ICT band is blue-shifted in random copolymers and observed at 675 nm in BSS10, at 659 nm in BSS20, and at 614 nm in BSS50.

Thin film absorption spectra are much similar to solution spectra, except the low energy (ICT) bands are red-shifted due to the increased conjugation and intermolecular interaction in the solid state. The reference BSS0 showed ICT band at 720 nm, which is shifted to 703 in BSS10, to 698 nm in BSS20, and to 668 nm in BSS0. The observed blue-shifting of ICT band in the solid state indicates that the chain planarity or/and rigidity is decreased in random copolymers due to the induced disorder by selenophene unit. The optical band gap (E_g^{opt}) of the new random copolymer was determined from the onset absorption band edge of thin film spectra. E_g^{opt} value is increased from 1.40 eV in reference BSS0 to 1.45 eV in BSS10 and BSS20 and to 1.50 eV in BSS50. We measured optical absorption for a thin film of donor polymer PBDB-T (Figure 7a), and the spectra showed strong absorption band in the visible region (at 450-700 nm) with absorption maxima at 600 nm and E_g^{opt} of 1.80 eV. The absorption profile of PBDB-T is perfectly complementary with the absorption bands of new random copolymers, also the PBDB-T:BSS*x* blend showed broad absorption bands in the region from 300 to 900 nm (Figure S5). The broad

and complementary absorption of D/A blend film is desirable for improving the light harvesting and therefore enhancing the photocurrent density (J_{sc}) of all-PSCs.[11]

The electronic structure of BSS*x* copolymers was investigated by carrying out the cyclic voltammetry (CV) on the thin films of the copolymer (Figure S4). The ferrocene/ferrocenium (Fc/Fc^+) redox couple was used as an internal standard by assigning absolute energy level of -4.8 eV versus vacuum level.[41] The observed onset reduction potentials of the copolymers from CV was used to determine the LUMO energy levels (LUMO = -(e E_{red}^{onset} (V vs Fc/Fc^+) + 4.8 eV)), similarly the oxidation potential was used to determine the HOMO energy levels (HOMO = -(e E_{oxd}^{onset} (V vs Fc/Fc^+) + 4.8 eV)). As shown in Figure 7b, all the polymers showed almost similar LUMO values in the range of -3.90-3.98 eV, suggesting that selenophene incorporation has a negligible effect on the electron-accepting strength of random copolymers. Except for BSS50, all the polymers showed identical HOMO level -5.83 eV. The CV scan of BSS50 did not show an oxidation peak up to 2 V, may be due to weak electron donating nature of copolymer. Thus, similar to reported in our prior work[6], we assume the HOMO energy level of BSS0 to be either at or lower lying than -6.0 eV. The literature reported HOMO and LUMO energy level of donor polymer PBDB-T is -5.33 V/-3.53 V, respectively.[42] These HOMO/LUMO energy levels provide sufficient energy offsets (> 0.3 eV) with each of BSS*x* copolymer acceptors and satisfying the prerequisite for efficient photoinduced electron transfer and hole transfer required for the photovoltaic device.

Wide-angle X-ray (XRD) measurement was performed on thermally annealed (130 °C for 10 min) drop-casted films of polymers on a glass substrate to characterize the molecular packing and bulk crystalline behavior of new random copolymers as a neat film. The corresponding XRD patterns are shown in Figure S7. XRD patterns of reference BSS0 sample showed an intense lamellar ordering (100) peak at $2\theta = 3.72°$ and a chain stacking peak (010) peak at $2\theta = 22.70°$

that corresponds to lamellar packing distance of 23.70 Å and a π-π stacking distance of 3.90 Å. For random copolymers, the lamellar (100) peak intensity and peak order were found to decrease at similar film processing conditions. The lamellar (100) peak was observed at 3.73° for BSS10, at 3.70° for BSS20, and at 3.75° for BSS50 that corresponds to the lamellar packing distances of 23.62 Å, 23.85 Å, 23.53 Å respectively. The π-π stacking distance was found to increase progressively from 3.90 Å in reference BSS0 to 3.95 Å in BSS10, to 3.98 Å in BSS20, and to 4.02 Å in BSS50, noticeably the π-π stacking (010) peak for BSS20 and BSS50 has become significantly broad. The increased stacking distance in the random copolymer was accounted for by the reduced backbone planarity due to the incorporation of selenophene.

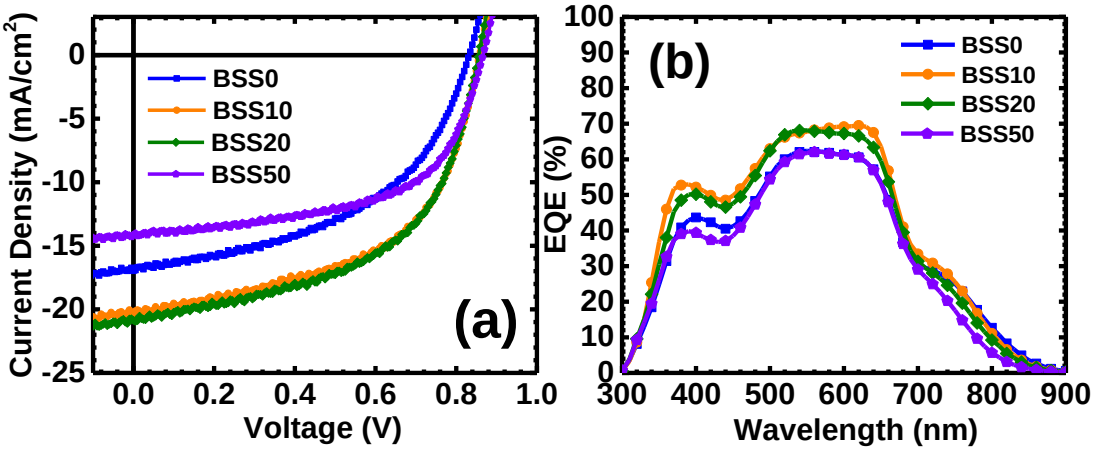

Figure 8. Current density (J_{sc})-Voltage (V) characteristics (a) EQE spectra (b) for optimal PBDB-T:BSS*x* all-polymer solar cells. All the blend of active layers were thermally annealed at 175 °C for 10 min.

The photovoltaic properties of new random copolymers (BSS*x*) as electron acceptor component and PBDB-T as electron donor component were investigated by fabricating and evaluating the all-PSC device with the inverted structure: ITO/ZnO/PEI/blend/MoO3/Ag, where polyethyleneimine (PEI) is a cathode interface layer.[43] The photovoltaic device measurements

were carried out under solar illumination of AM 1.5G simulated solar light at 100 mW/cm^2. The PBDB-T:BSS*x* all-polymer blend active layer were prepared under optimized conditions of blend ratio 1:0.6 (wt:wt), spin coating from chlorobenzene solution, and thermal annealing at 175 °C for 10 min without using any solvent additives or special post-processing treatment. All-PSC devices of reference PBDB-T:BSS0 blend also fabricated under similar conditions for comparison purpose. The current density-voltage (*J*-*V*) curves and the external quantum efficiency (EQE) spectra of all-PSC devices are given in Figure 8a and 8b respectively. The all-PSC device parameters, including the short-circuit current density (J_{sc}), the open-circuit voltage (V_{oc}), and fill factor (FF), and PCE, are summarized in Table 4.

Table 4. Photovoltaic Properties of Thermally Annealed (175 °C for 10 min) PBDB-T:BSS*x* (1:0.6 wt/wt) Blend Solar Cells.

polymer	J_{sc} (mA/cm^2)	V_{oc} (V)	FF	PCE_{max} (%)	PCE_{ave} (%)[a]
BSS0	16.87	0.82	0.45	6.83	6.27 (±0.24)
BSS10	20.02	0.86	0.52	9.49	8.96 (±0.27)
BSS20	19.70	0.86	0.54	9.58	9.14 (±0.26)
BSS50	14.19	0.86	0.58	7.51	7.14 (±0.30)

[a)] Average PCE values obtained from 15 or more separate devices.

The reference PBDB-T:BSS0 solar cell devices showed a maximum PCE of 6.83% with J_{sc} of 16.87 mA/cm^2, V_{oc} of 0.82, and FF 0.45. This performance is in good agreement with our previously reported all-PSC with similar blend active layer and under thermal annealing condition. Compared to the reference PBDB-T:BSS0 blend, the optimized all-PSC devices of random copolymers blends: PBDB-T:BSS10 and PBDB-T:BSS20, exhibited significantly enhanced photovoltaic performance. The PCE of 9.49% has been observed for BSS10 with J_{sc} of 20.02

mA/cm^2, V_{oc} of 0.86, FF 0.52. The PCE was further increased up to 9.58% in BSS20 with J_{sc} of 19.70 mA/cm^2, V_{oc} of 0.86, FF 0.54. The PCE enhancement was observed due to the overall improvement in the photovoltaic parameters (J_{sc}, V_{oc}, and FF), while photocurrent (J_{sc}) was much improved for both the copolymers. A device performance of PBDB-T:BSS50 blend was significantly lower as compared to the BSS10, and BSS20 with the maximum PCE of 7.50% (J_{sc} of 14.19 mA/cm^2, V_{oc} of 0.86, FF 0.58) was seen, this performance is still higher than reference blend device. The observed lower PCE value for BSS50 relative to the other random copolymers strongly suggests that further increase in the ratio of selenophene may not be helpful to improve the device performance; therefore, BSS10 and BBS20 are considered as optimum compositions. Overall, a higher photocurrent (J_{sc}) and FF value observed in BSS*x* blend device as compared to the reference sample indicates that random copolymers produce more compatible donor:acceptor blend due to their more flexible backbone.

It is well known that the use solvent additives and/or different post-processing treatments are beneficial to realize an optimum thin film morphology and high efficiency in PSCs.[44, 45] To test this fact, we systematically fabricated the solar cell devices of BSS*x* copolymers under different processing conditions, including drying of the active layer at room temperature, vacuum drying, thermal annealing at different temperature and use of processing additives. Representative *J*-*V* curves are depicted in Figure S8-S11, and the photovoltaic parameters are summarized in the Table S1-S4. Room temperature drying (25 °C) in either slow or fast rate as well as utilizing different processing additives (DPE, ODT, CN, and DIO) were found to be detrimental (or not much helpful) to the devices performance. Instead, simple thermal annealing at 175 °C for 10 min appeared to be the most effective technique to achieve optimized all-PSC devices for the random copolymer. We note that all recently reported random copolymer acceptor needs the extensive help

of solvent additives and/or tedious processing treatment to realize optimum thin film morphology.[24, 27, 31, 32] In stark contrast, the morphology optimization of all-PSC in BSS*x* random copolymer is achieved without using solvent additives and with relatively simple processing technique.

We screened a wide range of annealing temperatures (80-230 °C) to further investigate the thermal stability of BSS10 and BSS20-based all-PSC devices. As shown in Table S3, BSS10-based devices exhibited relatively stable V_{oc} values within ranges of 0.85-0.87 V. FF of devices were decreased slightly from 0.56 at 80°C to 0.52 at 175°C and then remains stable at a higher temperature (up to 200 °C). Although the FF is reduced from 80°C to 175°C, it is compensated by a significant enhancement in the photocurrent (J_{sc}) from 17.23 mA/cm^2 to 20.08 mA/cm^2, respectively, leading to an overall increase in the all-PSC device performance at 175°C. In the case of BSS20-based devices, the V_{oc} values (0.86) are quite stable up to 200°C (Table S4). FF of the device was reduced only from 0.55 at 80°C to 0.53 at 175°C, nonetheless again increased to 0.55 at 200 °C. Photocurrent (J_{sc}) was increased significantly from 17.55 mA/cm^2 at 80°C to 20.39 mA/cm^2 at 175°C and again decreased to 17.11 mA/cm^2 at 200°C. We note that even after thermal annealing at high temperature (200 °C), the overall PCE of BSS20-based devices is only decreased from 8.34% at 80 °C and 9.58% at 175 °C to 8.27% at 200 °C with the PCE loss ratio of ~1% and ~14% respectively. These results are pointing towards the excellent thermal stability of BSS20-based all-PSCs. To the best of our knowledge, the stable performance at high annealing temperature without using a solvent additive is not reported so far for random copolymers acceptor-based all-PSCs.

The EQE spectra of the optimum PBDB-T:BSS*x* blend devices are shown in Figure 8b. Copolymer BSS0, BSS10, and BSS20 blends exhibited photoresponse from a near infrared region

at around 885 nm which corresponds to the onset absorption of acceptor polymers to the ultraviolet region at approximately 300 nm. For BBS50, the photoresponse starts from 830 nm which is consistent with its thin film absorption spectra that exhibited a wider optical band gap (1.5 eV). A strong complementary absorption spectrum between donor and acceptor benefitted to the efficient photoinduced charge transfer processes in all the copolymer blends. Specifically, photoinduced electron transfer originating from PBDB-T donor polymer prevails in 450 – 650 nm region while photoinduced hole transfer stemming from acceptor polymers (BSS*x*) dominates in 350 – 450 nm and 680 – 850 nm. Although the EQE curve pattern is similar for all copolymers, the BSS10 and BSS20 blends have higher EQE than the BSS0 and BSS50 with the peak EQE values of about ~ 70% in the 500-650 nm region. This enhanced photoresponse of BSS10 and BSS20 copolymer blends corroborates the observed higher J_{sc} values in solar cells performance. The photocurrent obtained by integrating the EQE curves are lower than the J_{sc} measured from J-V curves with a mismatch within 15-30%. This large mismatch could be due to the synergic effect of the spectral mismatch between the simulated light source and the AM1.5 G solar spectrum as well as the lower absorption coefficient of these copolymers in the near-infrared region.

We note a few important outcomes of the present photovoltaic study. First we designed and developed for the first-time new series of electron accepting random copolymers for efficient all-PSCs. Second, the high-performance all-PSC devices are obtained by using relatively simple device fabrication process without using any solvent additives and/or additional post-processing treatments, which is beneficial for manufacturing all-PSCs by throughout the fabrication process. Third, the blend active layer morphology exhibited good thermal stability at high temperature, suggesting the thermal and mechanical robustness of random copolymer-based all-PSC for practical operation. Fourth, the photocurrent (20.02 mA/cm^2) and PCE (9.6%) observed in inverted

PBDB-T:BSS*x* blend devices are the highest observed so far for all-PSC based on the random copolymer acceptors.

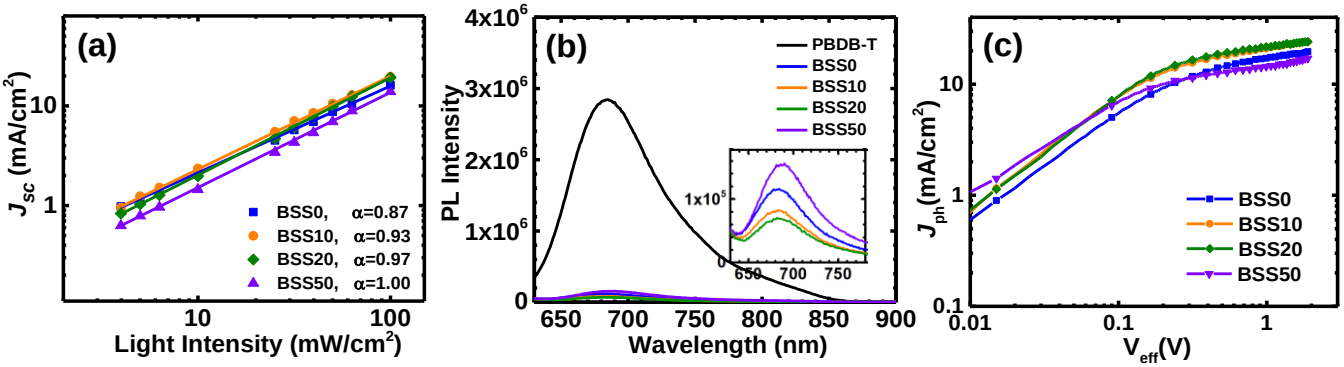

Figure 9. (a) J_{ph}-V_{eff} curves (b) PL spectra (600 nm excitation) of neat PBDB-T donor film and blend film. (c) J_{sc} dependence on light intensity for all-PSCs based on PBDB-T:BSS*x* blends (1:0.6 wt/wt).

To evaluate the photoinduced charge carrier generation and charge collection behavior in BSS*x*:PBDB-T blend devices, we analyzed the photocurrent density J_{ph} ($J_{ph} = J_L - J_D$) versus effective voltage V_{eff} ($V_{eff} = V_{bi} - V_a$) curves (Figure 9a), where J_L and J_D are the current densities under illumination, and dark conditions, respectively, and V_{bi} is the built-in-voltage or voltage when $J_{ph} = 0$ and V_a is the applied voltage. For all copolymers, J_{ph} saturates at high V_{eff} values of about 2V, resulting in a saturation photocurrent density (J_{sat}) of 23 mA/cm^2 in both BSS10 and BSS20-based devices, 16.7 mA/cm^2 in the BSS50 device, and 19 mA/cm^2 in BSS0 device. It can be concluded that the effective voltage is large enough to extract nearly all photogenerated free charges to the electrode at a saturation point.[46] Therefore, the G_{max} which represents a maximum photoinduced carrier generation rate can be estimated from the J_{sat}: ($G_{max} = J_{sat}/ q.L$), where q is the elementary charge and L is active layer thickness. Among the all-PSCs, copolymer BSS10 and BSS20 device showed highest value for G_{max} 15.0 x10^{27} m^{-3} s^{-1} and 15.5 x10^{27} m^{-3} s^{-1}, respectively,

while the BSS50 and BSS0 device yielded lower G_{max} values of 11.3 x10^{27} m^{-3} s^{-1} and 10.9 x10^{27} m^{-3} s^{-1}, respectively. The observed high G_{max} values imply that more efficient light absorption and exciton dissociation occurs in BSS10 and BSS20-based all-PSCs as compared other copolymer devices which are attributed to the enhanced thin-film UV-visible absorption of BSS10 and BSS20. These results further give supports to the observed increased J_{sc} for BSS10 and BSS20 devices than BSS50 and BSS0 devices. Next, we investigated the charge collection capacity of these blend devices by calculating the charge collection probability P (E, T) under short circuit condition. A higher value of P (E, T), 90.4% and 93.5% have been estimated for BSS10 and BSS20, respectively as compared to 89.3% in BSS0 and 84.8% in BSS50, which suggests that the charge collection process is more efficient in BSS10 and BSS20-based devices.

We also carried out the photoluminescence (PL) experiment to further understand the exciton dissociation and charge transfer in the PBDB-T:BSS*x* solar cell devices. The PL spectra of pristine PBDB-T thin film and after blending with the BSS*x* (1:0.6 wt/wt) copolymers are shown in Figure 9b. The donor polymer PBDB-T exhibits a broad PL spectrum which extends from 625 nm to 860 nm with a peak maximum at 690 nm. As compared to PBDB-T, the intensity of PL spectra of blend films is drastically decreased with relative quenching efficiency of 97% in BSS20, 96% in BSS10, 94% in BSS50, and 95% in BSS0. The strong quenching of PL spectra suggests that the photoinduced charge transfer is highly efficient in all copolymer-based devices. However, the slightly higher quenching of PL spectra in BBS10 and BSS20 blends as compared to BSS50 and BSS0 indicates that the BSS10 and BSS20 blend devices must have a highly interpenetrating polymer/polymer blend morphology with small phase-separated domains that enabled efficient exciton dissociation.

To gain insights into the charge recombination kinetics of the random copolymers all-PSC devices, we measure their current density (J_{sc}) as a function of an illumination intensity (P_{light}). As demonstrated in Figure 9c that the J_{sc} follows the expected power-law dependence on P_{light} ($J_{sc} \propto (P_{light})^{\alpha}$), where linearity ($\alpha = 1$) indicates weak carrier losses due to bimolecular recombination.[47] The slope of the fitted line in the J_{sc}-P_{light} plots gives rise to α value of 0.87 for reference BSS0 blend devices. Relative to the reference BSS0, random copolymer devices show higher α values of 0.93 in BSS10, 0.97 in BSS20, and 1.00 in BSS50, which indicates that the random copolymer-based devices have weak losses due to the bimolecular recombination as compared to BSS0. The higher α values further corroborate with the observed high FF values (0.52-0.58) in random copolymer-based devices than the reference PBDB-T:BSS0 blend device (0.45). Particularly, BSS50 copolymer with α values of 1 exhibited the highest FF of 0.58 in this series of the random copolymer.

Table 5. SCLC Charge Carrier Mobilities for Neat Film of Acceptor Polymers and in the Blends (PBDB-T:BSS*x*) Annealed at 175 ºC for 10 min.

Polymer	μ_e ($cm^2\ V^{-1}\ s^{-1}$)	μ_h ($cm^2\ V^{-1}\ s^{-1}$)	μ_h / μ_e
BSS0	3.49×10^{-5}	-	-
BSS10	1.60×10^{-4}	-	-
BSS20	2.42×10^{-4}	-	-
BSS50	5.35×10^{-5}	-	-
PBDB-T: BSS0	1.69×10^{-5}	1.89×10^{-4}	11.2
PBDB-T: BSS10	6.77×10^{-5}	5.33×10^{-4}	7.88
PBDB-T: BSS20	6.14×10^{-5}	4.43×10^{-4}	7.21
PBDB-T: BSS50	2.18×10^{-5}	6.28×10^{-5}	2.88

We examined the bulk charge carrier mobilities of the all-polymer blend films by using space charge limited current (SCLC) measurement; the blend films were prepared under similar conditions as used for solar cell devices. The free hole and electron mobilities were measured in device configuration of (ITO/PEDOT:PSS/Active layer/MoO_3/Ag) and (ITO/ZnO/PEI/Active layer/LiF/Al), respectively. SCLC measurement of neat films of new copolymer acceptors was also investigated to understand the effect of selenophene incorporation on the charge transport properties of random copolymers. The *J-V* curve and SCLC fittings of the data are included in the Figure S13 (for blend devices) and Figure S13 (for neat films), while the mobilities are summarized in Table 5.

For a neat film of acceptor polymers, the reference BSS0 showed electron mobility (μ_e) of 3.49 x 10^{-5} cm^2/Vs. In contrast, the electron mobilities were significantly enhanced for BSS10 and BSS20 copolymer with μ_e increase about 5-fold in BSS10 (μ_e = 1.60 x 10^{-4} cm^2/Vs) and 7-fold (μ_e = 2.42 x 10^{-4} cm^2/Vs) in BSS20. For BSS50 the mobility was only slightly increased to (μ_e = 5.35 x 10^{-4} cm^2/Vs). The observed high increase of the electron mobility indicates that random copolymer has favorable face-on oriented molecular packing (discussed later in GIXRD section) which leads to efficient electron transport. In the case of blend devices, overall the electron mobilities are decreased than the neat films, nevertheless similar to the neat films in blend random copolymers showed enhanced electron mobility. The electron mobilities increased from 1.69 x 10^{-5} cm^2/Vs in BSS0 to 6.77 x 10^{-5} cm^2/Vs in BSS10 to 6.14 x 10^{-5} cm^2/Vs in BSS20, and to 2.18 x 10^{-5} cm^2/Vs in BSS50. Similarly, the hole mobilities are also enhanced by 2.8-fold in BSS10 (5.33 x 10^{-4} cm^2/Vs) and 2.3-fold in BSS20 (4.43 x 10^{-4} cm^2/Vs) as compared to BSS0 (1.89 x 10^{-4} cm^2/Vs) blend device, except the hole mobility is decreased to 6.28 x 10^{-5} cm^2/Vs for BSS50. The observed substantial increase of mobilities in random copolymer suggests that the PBDB-T:BSS*x*

system have more favorable bulk morphology for efficient charge transport than the reference BBS0: PBDB-T blend.

We further analyze the (μ_h/μ_e) ratio of mobility and observed that the reference BSS0 blend device has highest unbalanced mobilities (μ_h/μ_e = 11.2). In contrast, random copolymers showed more balanced charge transport with (μ_h/μ_e) of 7.88 in BSS10, 7.21 in BSS20, and 2.88 in BSS50. We note that the balanced (μ_h/μ_e) ratio and high charge carrier mobilities are highly desirable to reduce the bimolecular recombination in solar cell devices; thereby maximize the photocurrent and FF value.[31, 48] New random copolymer exhibits high electron and hole mobilities and more balanced charge transport than the reference BBS0 which agrees well with their observed high J_{sc} and FF in all-PSCs. However, the (μ_h/μ_e) ratio is still high in random copolymer blend devices which is the reason for the overall lower FF.

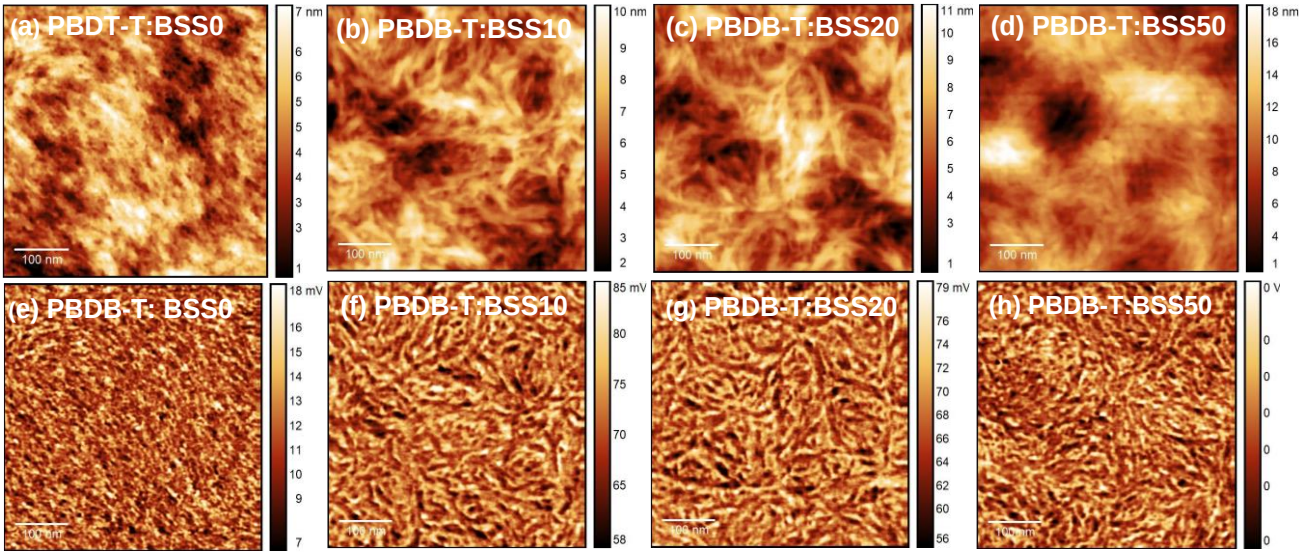

Figure 10. AFM height (a, b, c, and d) and phase (d, e, f, and h) images (500 nm x 500 nm) of the surfaces of PBDB-T:BSS*x* blend devices. The scale bars are 100 nm.

We characterize the thin film surface morphology of PBDB-T:BSS*x* blend devices by tapping-mode atomic force microscopy (AFM). The surface images of neat film of polymer acceptors were also recorded for comparison purpose. AFM height and phase images of neat films are shown in Figure S12. All copolymer acceptor showed identical densely packed granular morphology. In the case of blend films, there are no striking differences observed in the morphology of BSS0 blend versus neat film. In contrast, random copolymer blends manifested fiber like phase separated morphology (Figure 10). Moreover, the domain size of BSS0 of approximately 20 nm is slightly higher than that of other copolymers which average around 10-15 nm. For random copolymers, in the transition of neat to blend film, not only the morphological pattern changed, but the surface roughness also is escalated deduced from increasing values of RMS; 1.11 nm in neat film to 1.47 nm in blend film for BSS10, 1.03 nm in neat film to 1.74 nm in blend film for BSS20, and 0.78 nm in neat film to 2.54 nm in blend film for BSS50 . On the other hand, the RMS value for BSS0 is closely similar for the neat film (0.90 nm) and blend (0.99 nm). Thus, from AFM analysis, we can infer that the random copolymers blends have highly intermixed domains of donor and acceptor polymer with suppressed macroscopic phase separation than the reference BSS0 blend.

To investigate the influence of higher annealing temperature on the surface morphology of PBDB-T:BSS10 and PBDB-T:BSS20 blend films, we recorded AFM images of blend films annealed at 200 °C and 230 °C. As shown in Figure S15 both the PBDB-T:BSS10 and PBDB-T:BSS20 blend showed fiber like phase separated morphology which is closely similar to the morphology observed for blend films annealed at 175 °C. Moreover, the RMS values are only slightly changed over different temperature (Table S5).

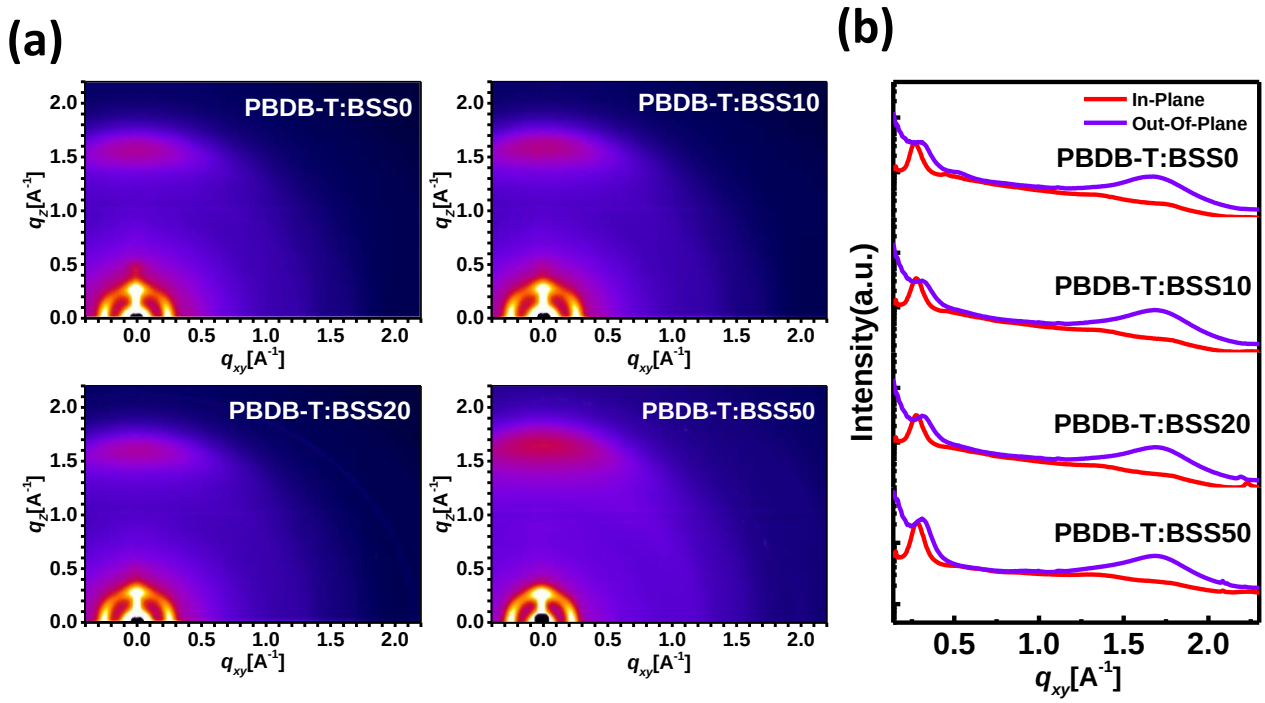

Figure 11. (a) 2D-GIWAXS images of PBDB-T:BSS*x* blend films. Line cuts of GIWAXS patterns (b) (red pattern: in-plane; violet pattern: out-of-the-plane).

Thin film morphology of neat films of copolymers and their optimum blend with PBDB-T donor polymer were characterized by 2D-Grazing incident wide-angle X-ray scattering (2D-GIWAXS) measurements. 2D-GIWAXS pictures and line-cuts profile for neat copolymers and their blends films are shown in Figure S16 and Figure 11, respectively. The neat film of reference BSS0 copolymer showed (100) diffuse ring with sharp (001) (200) peaks along in-plane (IP) direction, and (100) (010) peak along the out-of-the-plane (OOP) direction. Such pattern in GIWAXS could observe due to the rigid backbone of polymer likely oriented along in-plane.[32, 49] For copolymers, the (100) peak in IP direction was located at q_{xy} = 0.25 Å^{-1} which resembles to the BSS0, however, interestingly the (001) peak at q_{xy} = 0.44 Å^{-1} become diffused and less intense in BSS10 and even disappeared completely in BSS20 and BSS50. Similarly, (200) peak at q_z = 0.53 Å^{-1} as observed for BSS0 in OOP direction become less intense or disappeared in random

copolymers. The disappearance of few higher order lamellar peaks both in IP and OOP direction suggest the substantial reduction in crystallinity along with a significant change in the molecular orientations in the random copolymers. All random copolymers showed well defined (010) reflection from π-π stacking in OOP, and corresponding (100) reflection from lamellar stacking is located (IP), without a diffuse ring. This kind of mirrored reflection between (100) and (010) is typically observed due to the more face-on orientation of polymer relative to the substrate.[49] The crystal correlation length (CCL) determined from Scherrer equation analysis of (100) peak was found to be decreased progressively from 17.4 nm in BSS0 to 15.1 nm in BSS10, to 14.7 nm in BSS20, and to 12.1 nm in BSS50 (Table S6). Our 2D-GIWAXS measurement on the donor PBDB-T films agree well with a prior report, OOP (010) peak for π-π stacking is observed at q_z = 1.68 Å^{-1}, and the lamellar peak (100) at q_{xy} = 0.28 Å^{-1} is located in the IP cut.[50] The calculated (L_c) value for PBDB-T is 5.5 nm, which is ideal as a component to be paired with a more crystalline one in all-PSC.[24]

Blend film of random copolymers showed broad (100) peak at q_{xy} = 0.27 Å^{-1} in IP direction and the (010) peak at q_z = 1.69 Å^{-1} in OPP direction (Figure 11). The (100) peak observed at q_z = 0.31 Å^{-1} in OOP direction is broadened, weaken in intensity, and shifted to a higher q value as compared to their neat films (q_z = 0.28 Å^{-1}). These observations altogether imply that the crystallinity of random copolymers is decreased in blend film, while face-on molecular orientation has significantly improved. In contrast, the reference BSS0 polymer showed some edge-on orientated chains on the substrate as suggested by the appearance of (200) peak in OOP direction, which also indicates more crystalline nature and less miscibility of BSS0 chains in the blend as compared to new random copolymers. The (100) peak is for donor and acceptor is overlapped in blend which makes it difficult to estimate the CCL values of each component, nonetheless overall

CCL values were smaller (BSS10 = 6.4 nm, BSS20 = 6.0 nm, BSS50 = 6.8, and BSS0 = 6.7 nm) than observed in the neat films of acceptor copolymer, suggesting that crystalline domain size is much reduced in the blend. Overall, the 2D-GIWAXS results show that the molecular disorder created in random copolymer due to selenophene incorporation has been noticeably beneficial in improving the nanomorphology of all-PSC blends. As compared to reference high crystalline BSS0 polymer, the random copolymer with less crystalline nature showed favorable morphology with improved face-on molecular orientation, small crystalline domain sizes, enhanced donor/acceptor mixing in blend film, which correlates well with the observed high photocurrent and FF of random copolymer all-PSCs.

3.4 CONCLUSIONS

We have synthesized a series of new semiconducting random copolymers (BSS*x*) by introducing different mole percentage of selenophene into *n*-type NDI-biselenophene (BSS0) polymer backbone. The resulting copolymers were characterized for their thermal, optical, electrochemical, and bulk charge transport properties and evaluated as an electron acceptor in all-PSCs. Thin-film of BSS10 and BSS20 copolymers having 10% and 20% selenophene unit, respectively showed enhanced ICT absorption, reduced crystallinity, and higher bulk electron mobilities. Moreover, when combined with PBDB-T donor polymer they form a miscible blend with reduced domain sizes, favorable morphology with improved face-on orientations, and symmetric charge transport. As results, both BSS10 and BSS20 all-PSC devices exhibited higher PCE of 9.5% and 9.6%, respectively with higher photocurrent (20.02 mA/cm^2 and 19.70 mA/cm^2) which are among the best observed for all-PSC. More importantly, these high performing all-PSCs are fabricated without using any solvent additives or/and additional post-processing treatments, revealing the facile all-PSC morphology optimization with random copolymers. Furthermore,

BSS20-based all-PSC devices showed good thermal stability with ~ 99% (at 80 °C) of initial PCE was maintained after thermal annealing at 200 °C. Our work demonstrates that new random copolymers are promising alternatives to the current *n*-type polymers in term of PCE, while the new copolymer acceptor additionally offers solvent additive free thermally stable all-PSCs which will make the future device fabrication process more simple and scalable for practical application of all-PSCs.

3.5 REFERENCES

(1) Halls, J. J. M.; Walsh, C. A.; Greenham, N. C.; Marseglia, E. A.; Friend, R. H.; Moratti, S. C.; Holmes, A. B., Efficient photodiodes from interpenetrating polymer networks. *Nature* **1995,** *376*, 498.

(2) Jenekhe, S. A.; Yi, S., Efficient photovoltaic cells from semiconducting polymer heterojunctions. *Appl.Phys. Lett.* **2000,** *77*, 2635-2637.

(3) Facchetti, A., Polymer donor–polymer acceptor (all-polymer) solar cells. *Mater. Today* **2013,** *16*, 123-132.

(4) Benten, H.; Mori, D.; Ohkita, H.; Ito, S., Recent research progress of polymer donor/polymer acceptor blend solar cells. *J. Mater. Chem. A* **2016,** *4*, 5340-5365.

(5) Kang, H.; Lee, W.; Oh, J.; Kim, T.; Lee, C.; Kim, B. J., From Fullerene–Polymer to All-Polymer Solar Cells: The Importance of Molecular Packing, Orientation, and Morphology Control. *Acc. Chem. Res.* **2016,** *49*, 2424-2434.

(6) Hwang, Y.-J.; Courtright, B. A. E.; Ferreira, A. S.; Tolbert, S. H.; Jenekhe, S. A., 7.7% Efficient All-Polymer Solar Cells. *Adv. Mater.* **2015,** *27*, 4578-4584.

(7) Lu, L.; Zheng, T.; Wu, Q.; Schneider, A. M.; Zhao, D.; Yu, L., Recent Advances in Bulk Heterojunction Polymer Solar Cells. *Chem. Rev.* **2015,** *115*, 12666-12731.

(8) Kim, T.; Kim, J.-H.; Kang, T. E.; Lee, C.; Kang, H.; Shin, M.; Wang, C.; Ma, B.; Jeong, U.; Kim, T.-S.; Kim, B. J., Flexible, highly efficient all-polymer solar cells. **2015,** *6*, 8547.

(9) Lin, Y.; Dong, S.; Li, Z.; Zheng, W.; Yang, J.; Liu, A.; Cai, W.; Liu, F.; Jiang, Y.; Russell, T. P.; Huang, F.; Wang, E.; Hou, L., Energy-effectively printed all-polymer solar cells exceeding 8.61% efficiency. *Nano Energy* **2018,** *46*, 428-435.

(10) Earmme, T.; Hwang, Y.-J.; Murari, N. M.; Subramaniyan, S.; Jenekhe, S. A., All-Polymer Solar Cells with 3.3% Efficiency Based on Naphthalene Diimide-Selenophene Copolymer Acceptor. *J. Am. Chem. Soc.* **2013,** *135*, 14960-14963.

(11) Gao, L.; Zhang, Z.-G.; Xue, L.; Min, J.; Zhang, J.; Wei, Z.; Li, Y., All-Polymer Solar Cells Based on Absorption-Complementary Polymer Donor and Acceptor with High Power Conversion Efficiency of 8.27%. *Adv. Mater.* **2016,** *28*, 1884-1890.

(12) Fan, B.; Ying, L.; Zhu, P.; Pan, F.; Liu, F.; Chen, J.; Huang, F.; Cao, Y., All-Polymer Solar Cells Based on a Conjugated Polymer Containing Siloxane-Functionalized Side Chains with Efficiency over 10%. *Adv. Mater.* **2017,** *29*, n/a-n/a.

(13) Fan, B.; Ying, L.; Wang, Z.; He, B.; Jiang, X.-F.; Huang, F.; Cao, Y., Optimisation of processing solvent and molecular weight for the production of green-solvent-processed all-polymer solar cells with a power conversion efficiency over 9%. *Energy & Environ Sci.* **2017,** *10*, 1243-1251.

(14) Li, Z.; Xu, X.; Zhang, W.; Meng, X.; Genene, Z.; Ma, W.; Mammo, W.; Yartsev, A.; Andersson, M. R.; Janssen, R. A. J.; Wang, E., 9.0% power conversion efficiency from ternary all-polymer solar cells. *Energy & Environ Sci.* **2017,** *10*, 2212-2221.

(15) Guo, Y.; Li, Y.; Awartani, O.; Han, H.; Zhao, J.; Ade, H.; Yan, H.; Zhao, D., Improved Performance of All-Polymer Solar Cells Enabled by Naphthodiperylenetetraimide-Based Polymer Acceptor. *Adv. Mater.* **2017,** *29*, n/a-n/a.

(16) Zhao, J.; Li, Y.; Yang, G.; Jiang, K.; Lin, H.; Ade, H.; Ma, W.; Yan, H., Efficient organic solar cells processed from hydrocarbon solvents. *Nat. Energy* **2016,** *1*, 15027.

(17) Shaoqing, Z.; Yunpeng, Q.; Jie, Z.; Jianhui, H., Over 14% Efficiency in Polymer Solar Cells Enabled by a Chlorinated Polymer Donor. *Adv. Mater.* **2018,** *30*, 1800868.

(18) Li, S.; Ye, L.; Zhao, W.; Yan, H.; Yang, B.; Liu, D.; Li, W.; Ade, H.; Hou, J., A Wide Band Gap Polymer with a Deep Highest Occupied Molecular Orbital Level Enables 14.2% Efficiency in Polymer Solar Cells. *J. Am. Chem. Soc.* **2018,** *140*, 7159-7167.

(19) Hwang, Y.-J.; Li, H.; Courtright, B. A. E.; Subramaniyan, S.; Jenekhe, S. A., Nonfullerene Polymer Solar Cells with 8.5% Efficiency Enabled by a New Highly Twisted Electron Acceptor Dimer. *Adv. Mater.* **2016,** *28*, 124-131.

(20) Hwang, Y.-J.; Ren, G.; Murari, N. M.; Jenekhe, S. A., n-Type Naphthalene Diimide–Biselenophene Copolymer for All-Polymer Bulk Heterojunction Solar Cells. *Macromolecules* **2012,** *45*, 9056-9062.

(21) Jung, J.; Lee, W.; Lee, C.; Ahn, H.; Kim, B. J., Controlling Molecular Orientation of Naphthalenediimide-Based Polymer Acceptors for High Performance All-Polymer Solar Cells. *Adv. Energy Mater.* **2016,** *6*, n/a-n/a.

(22) Lee, W.; Lee, C.; Yu, H.; Kim, D.-J.; Wang, C.; Woo, H. Y.; Oh, J. H.; Kim, B. J., Side Chain Optimization of Naphthalenediimide–Bithiophene-Based Polymers to Enhance the Electron Mobility and the Performance in All-Polymer Solar Cells. *Adv. Funct. Mater.* **2016,** *26*, 1543-1553.

(23) Kang, T. E.; Kim, K.-H.; Kim, B. J., Design of terpolymers as electron donors for highly efficient polymer solar cells. *J. Mater. Chem. A* **2014,** *2*, 15252-15267.

(24) Hwang, Y.-J.; Earmme, T.; Courtright, B. A. E.; Eberle, F. N.; Jenekhe, S. A., n-Type Semiconducting Naphthalene Diimide-Perylene Diimide Copolymers: Controlling Crystallinity, Blend Morphology, and Compatibility Toward High-Performance All-Polymer Solar Cells. *J. Am. Chem. Soc.* **2015,** *137*, 4424-4434.

(25) An, Y.; Oh, J.; Chen, S.; Lee, B.; Lee, S. M.; Han, D.; Yang, C., Effects of incorporating different chalcogenophene comonomers into random acceptor terpolymers on the morphology and performance of all-polymer solar cells. *Polym. Chem.* **2018,** *9*, 593-602.

(26) Kim, Y.; Cho, H.-H.; Kim, T.; Liao, K.; Kim, B. J., Terpolymer approach for controlling the crystalline behavior of naphthalene diimide-based polymer acceptors and enhancing the performance of all-polymer solar cells. *Polymer Journal* **2016,** *48*, 517.

(27) Sharma, S.; Kolhe, N. B.; Gupta, V.; Bharti, V.; Sharma, A.; Datt, R.; Chand, S.; Asha, S. K., Improved All-Polymer Solar Cell Performance of n-Type Naphthalene Diimide–Bithiophene P(NDI2OD-T2) Copolymer by Incorporation of Perylene Diimide as Coacceptor. *Macromolecules* **2016,** *49*, 8113-8125.

(28) Li, X.; Sun, P.; Wang, Y.; Shan, H.; Xu, J.; You, C.; Xu, Z.-x.; Chen, Z.-K., Design of three-component randomly incorporated copolymers as non-fullerene acceptors for all-polymer solar cells. *Polym. Chem.* **2016,** *7*, 2230-2238.

(29) Deng, P.; Ho, C. H. Y.; Lu, Y.; Li, H.-W.; Tsang, S.-W.; So, S. K.; Ong, B. S., Naphthalene diimide-difluorobenzene-based polymer acceptors for all-polymer solar cells. *Chemical Communications* **2017,** *53*, 3249-3252.

(30) Wang, E.; Hou, L.; Wang, Z.; Hellström, S.; Zhang, F.; Inganäs, O.; Andersson, M. R., An Easily Synthesized Blue Polymer for High-Performance Polymer Solar Cells. *Adv. Mater.* **2010,** *22*, 5240-5244.

(31) Li, Z.; Xu, X.; Zhang, W.; Meng, X.; Ma, W.; Yartsev, A.; Inganäs, O.; Andersson, M. R.; Janssen, R. A. J.; Wang, E., High Performance All-Polymer Solar Cells by Synergistic Effects of Fine-Tuned Crystallinity and Solvent Annealing. *J. Am. Chem. Soc.* **2016,** *138*, 10935-10944.

(32) Liu, X.; Zhang, C.; Duan, C.; Li, M.; Hu, Z.; Wang, J.; Liu, F.; Li, N.; Brabec, C. J.; Janssen, R. A. J.; Bazan, G. C.; Huang, F.; Cao, Y., Morphology Optimization via Side Chain Engineering Enables All-Polymer Solar Cells with Excellent Fill Factor and Stability. *J. Am. Chem. Soc.* **2018,** *140*, 8934-8943.

(33) Earmme, T.; Hwang, Y.-J.; Subramaniyan, S.; Jenekhe, S. A., All-Polymer Bulk Heterojuction Solar Cells with 4.8% Efficiency Achieved by Solution Processing from a Co-Solvent. *Adv. Mater.* **2014,** *26*, 6080-6085.

(34) Ye, L.; Jiao, X.; Zhao, W.; Zhang, S.; Yao, H.; Li, S.; Ade, H.; Hou, J., Manipulation of Domain Purity and Orientational Ordering in High Performance All-Polymer Solar Cells. *Chem. Mater.* **2016,** *28*, 6178-6185.

(35) Kang, H.; Kim, K.-H.; Choi, J.; Lee, C.; Kim, B. J., High-Performance All-Polymer Solar Cells Based on Face-On Stacked Polymer Blends with Low Interfacial Tension. *ACS Macro Letters* **2014,** *3*, 1009-1014.

(36) Shi, G.; Yuan, J.; Huang, X.; Lu, Y.; Liu, Z.; Peng, J.; Ding, G.; Shi, S.; Sun, J.; Lu, K.; Wang, H.-Q.; Ma, W., Combinative Effect of Additive and Thermal Annealing Processes Delivers High Efficiency All-Polymer Solar Cells. *J. Phys. Chem. C* **2015,** *119*, 25298-25306.

(37) Tremolet de Villers, B. J.; O'Hara, K. A.; Ostrowski, D. P.; Biddle, P. H.; Shaheen, S. E.; Chabinyc, M. L.; Olson, D. C.; Kopidakis, N., Removal of Residual Diiodooctane Improves Photostability of High-Performance Organic Solar Cell Polymers. *Chem. Mater.* **2016,** *28*, 876-884.

(38) Ye, L.; Jing, Y.; Guo, X.; Sun, H.; Zhang, S.; Zhang, M.; Huo, L.; Hou, J., Remove the Residual Additives toward Enhanced Efficiency with Higher Reproducibility in Polymer Solar Cells. *J. Phys. Chem. C* **2013,** *117*, 14920-14928.

(39) Marcel, S.; Daniel, D.; Johannes, F.; Steffen, R.; Robert, S.; Burkhard, S.; Zhihua, C.; Ullrich, S.; Norbert, K.; Antonio, F.; Dieter, N., Influence of Aggregation on the Performance of All-Polymer Solar Cells Containing Low-Bandgap Naphthalenediimide Copolymers. *Adv. Energy Mater.* **2012,** *2*, 369-380.

(40) Hwang, Y.-J.; Murari, N. M.; Jenekhe, S. A., New n-type polymer semiconductors based on naphthalene diimide and selenophene derivatives for organic field-effect transistors. *Polym. Chem.* **2013,** *4*, 3187-3195.

(41) Pavlishchuk, V. V.; Addison, A. W., Conversion constants for redox potentials measured versus different reference electrodes in acetonitrile solutions at 25°C. *Inorganica Chimica Acta* **2000,** *298*, 97-102.

(42) Li, S.; Ye, L.; Zhao, W.; Zhang, S.; Mukherjee, S.; Ade, H.; Hou, J., Energy-Level Modulation of Small-Molecule Electron Acceptors to Achieve over 12% Efficiency in Polymer Solar Cells. *Adv. Mater.* **2016,** *28*, 9423-9429.

(43) Courtright, B. A. E.; Jenekhe, S. A., Polyethylenimine Interfacial Layers in Inverted Organic Photovoltaic Devices: Effects of Ethoxylation and Molecular Weight on Efficiency and Temporal Stability. *ACS Appl. Mater. Interfaces* **2015,** *7*, 26167-26175.

(44) Peet, J.; Kim, J. Y.; Coates, N. E.; Ma, W. L.; Moses, D.; Heeger, A. J.; Bazan, G. C., Efficiency enhancement in low-bandgap polymer solar cells by processing with alkane dithiols. *Nature Materials* **2007,** *6*, 497.

(45) Yuan, J.; Xu, Y.; Shi, G.; Ling, X.; Ying, L.; Huang, F.; Lee, T. H.; Woo, H. Y.; Kim, J. Y.; Cao, Y.; Ma, W., Engineering the morphology via processing additives in multiple all-polymer solar cells for improved performance. *J. Mater. Chem. A* **2018,** *6*, 10421-10432.

(46) Mori, D.; Benten, H.; Okada, I.; Ohkita, H.; Ito, S., Highly efficient charge-carrier generation and collection in polymer/polymer blend solar cells with a power conversion efficiency of 5.7%. *Energy & Environ Sci.* **2014,** *7*, 2939-2943.

(47) Schilinsky, P.; Waldauf, C.; Brabec, C. J., Recombination and loss analysis in polythiophene based bulk heterojunction photodetectors. *Appl.Phys. Lett.* **2002,** *81*, 3885-3887.

(48) Proctor, C. M.; Kuik, M.; Nguyen, T.-Q., Charge carrier recombination in organic solar cells. *Progress in Polymer Science* **2013,** *38*, 1941-1960.

(49) Long, Y.; Xuechen, J.; Meng, Z.; Shaoqing, Z.; Huifeng, Y.; Wenchao, Z.; Andong, X.; Harald, A.; Jianhui, H., Manipulating Aggregation and Molecular Orientation in All-Polymer Photovoltaic Cells. *Adv. Mater.* **2015,** *27*, 6046-6054.

(50) Xu, S. j.; Zhou, Z.; Liu, W.; Zhang, Z.; Liu, F.; Yan, H.; Zhu, X., A Twisted Thieno[3,4-b]thiophene-Based Electron Acceptor Featuring a 14-π-Electron Indenoindene Core for High-Performance Organic Photovoltaics. *Adv. Mater.* **2017,** *29*, 1704510.

Chapter 4. ENGINEERING THE CATHODE INTERFACE TO ENHANCE THE PERFORMANCE OF ALL-POLYMER SOLAR CELLS

4.1 INTRODUCTION

Interfacial engineering has contributed to the compelling advances in the performance of organic electronics.[10] In particular, this strategy has significantly developed the performance of all-polymer solar cells (all-PSCs), which have attracted great attention for enhanced light absorption, lightweight, flexibility, the possibility of large-scale roll-to-roll printing at low cost as next-generation light harvesting technology.[4–6] By insertion of interlayers, the device can have benefits of better device stability from the penetration of water and oxygen, altering work function by the formation of a dipole moment for ohmic contact, energy level alignment establishing Fermi level pinning, selective blocking of hole and electron for efficient charge transport, passivation charge-trap sites, enhancing light absorption as optical spacer, and protection active layer from the metal ion diffusion during the thermal evaporation, resulting in improved device performance.[11–14] In the way of the insertion of interlayers between the active layer and each electrode, many materials such as metal salts, metal-oxide, organic materials have been applied and based on material properties and one's research purpose, either solution process or thermal evaporation have been selected. [11–14] However, ultimately solution process as compared to thermal evaporation of metal, which requires a lot of cost and energy, will be preferred in the aspects of processing cost and steps.

In conventional device structure, various research has been carried out for new electron-transport layers (ETLs) as cathode buffer layer, while PEDOT:PSS has been dominant hole

transport layer due to their appropriate work function, good transparency, high conductivity, and commercialization.[13,14] Instead of LiF which requires thermal evaporation method, PFN and their derivatives as water/alcohol soluble conjugated polymers have been widely used for solution processed ETLs for all-PSCs as the success has been proved in polymer light emitting diodes (PLEDs) for facilitating charge injection.[15–17] Likewise, there have also been some studies for organic photovoltaic cells with small-molecule ELTs of BCP and BPhen by thermal evaporation or forming a hybrid cathode with the inorganic semiconductor in PCBM system.[18–21] High electron mobility, deep HOMO, and transparency in the visible range of BCP and BPhen as ETLs facilitate the improvement of PLEDs. [22–25] Moreover, our lab has reported the various solution-processed ETLs with high-performance PLEDs.[22–25]

In this Chapter, I report a comparative study for the first time that 4,7-Diphenyl-1,10-phenanthroline (BPhen), 1,3-Bis[3,5-di(pyridin-3-yl)phenyl]benzene (BmPyPhB), and 1,3,5-Tri[(3-pyridyl)-phen-3-yl]benzene (TmPyPB) can be used as solution processed ETLs via simple spin-coating in all-PSCs. To evaluate the effects of solution-processed new-ETLs (BPhen, BmPyPhB, and TmPyPB), we systematically investigated a series of cathode case with Al, LiF/Al, Formic Acid(FA)/Al, PFN-Br/Al, BPhen/Al of all-PSCs. Besides, we further studied the cases of doped electron transport materials (ETMs) with alkali metal salt (Cs_2CO_3) for BPhen, BmPyPhB, and TmPyPB ETLs. We observed new-ETLs improved the short-circuit current (J_{sc}) as compared to Al, LiF/Al, and PFN-Br/Al with stable open circuit voltage (V_{oc}) of 0.85, but with a reduced fill factor (FF) of 0.48. We also found that the formic acid solution used as a solvent for new-ETLs could penetrate the active layer without any damage and dope the PEDOT:PSS. This results can be reflected in the case of FA/Al study, showing improved short-circuit current by comparison with Al, LiF/Al, and PFN-Br/Al cases. While high conductive and deep HOMO of new-ETLs and

doped PEDOT:PSS from the interaction of formic acid solution can enhance the photocurrent, the low fill factor of all-PSCs was caused.[26–28] The low fill factors of each new-ETL were also exposed in the charge collection probability calculation, and the short-circuit current density as a function of illumination intensity analysis. The surface morphologies of each ETL were studied by atomic force microscopy (AFM) imaging, and we found the trend of being reduced RMS with new-ETLs, which can help to make better contact with the Al electrode. Although new-ETLs processed by BPhen, BmPyPhB, and TmPyPB showed remarkable improvement for photocurrent, still it requires further detail studies. However, we believe it is worth trying new solution processable ETLs to develop efficient ETLs and improve the all-PSCs.

4.2 Experiment Section

Materials. The donor polymer PBDB-T (Mn = 62 kDa, Đ = 1.90) was purchased from Brilliant Matters Organic electronics (Quebec, Canada) and was used as received. The Acceptor polymer BSS10 was synthesized in our Lab. 4,7-diphenyl-1,10-phenanthroline (BPhen, 99%, sublimed grade), cesium carbonate (Cs 2 CO 3 , 99.9% trace metals basis), chlorobenzene (anhydrous, 99.8%) were purchased from Sigma-Aldrich Co. 1,3,5-Tris(m-pyrid-3-yl-phenyl)benzene (TmPyPB), and 1,3-bis(3,5-di(pyridine-3-yl)phenyl)benzene (BmPyPB) were purchased from Luminescence Technology (LumTec) Co., Taiwan. Formic acid, 88% (Certified ACS) was purchased from Fisher Chemical. PFN-Br was obtained from Alex Jen group, the University of Washington, WA, United Stated of America. A solution of PEDOT:PSS (poly-(ethylenedioxythiophene):polystyrenesulfonate, Heraeus Clevios™ AI 4083) dispersed in water was purchased from Ossila, United Kingdom. All purchased chemicals were used as received without further purification.

Fabrication and characterization of all-Polymer Solar Cells. All-polymer solar cells were fabricated with a conventional structure of ITO/PEDOT:PSS/Blend/ETLs/Al. ITO-coated substrates (15 Ω/□, Shanghai B. Tree Tech. Consult Co., Ltd., Shanghai, China) were cleaned sequentially in ultrasonic baths of acetone and isopropanol for 30 min, dried using nitrogen gas and followed by 10 min of O2 plasma cleaning. Right after the O2 plasma cleaning, the 30 nm thick PEDOT:PSS (Heraeus Clevios™ AI 4083) was spin-coated onto the ITO-coated substrates at 4000 rpm for 40 s and annealed at 150 °C for 10 min in air. The solution for each PBDB-T: BSS10 blend (1:0.6 wt/wt) was prepared in chlorobenzene, mixed and stirred overnight at 80 °C in the glove box. The blend solution was spin-coated at 1000 rpm for 50 s, followed by thermal annealing at 175 °C for 10 min. All the active layers had a thickness of 100 ± 5 nm. For each ETL, LiF (1 nm) was thermally deposited at a pressure of < 2 x 10-6 torr, and PFN-Br solution (0.5 mg/ml) dissolved in methanol was spin-coated onto the active layer at 4000 rpm for 40 s in the glove box. Small-molecule electron-transport materials (BPhen, BmPyPhB, and TmPyPB) were co-dissolved with alkali metal-salt (Cs_2CO_3) in formic acid and spin-coated onto the active layer at 7000 rpm for 40 s. After forming each ETL, thermally evaporated Al cathode (100 nm) was deposited onto the ETLs. Four pixels, each with an active area of 3 mm^2 were fabricated per ITO substrates. After evaporation of Al cathode, the photovoltaic cells were tested under AM 1.5 G solar illumination at 100 mW cm^2 in ambient air by using a solar simulator (Model 16S, Solar Light Co., Philadelphia, PA) with a 200W Xenon Lamp Power Supply (Model XPS 200, Solar Light Co., Philadelphia, PA) calibrated by NREL certified Si photodiode (Model 1787-04, Hamamatsu Photonics K.K., Japan) and a HP4155A semiconductor parameter analyzer (Yokogawa Hewlett Packard, Japan). After the J-V measurement, the external quantum efficiency (EQE) was measured by using a solar cell quantum efficiency measurement system (Model

QEX10, PV Measurements, Inc., Boulder, CO) with a 2 mm (2 mm × 1 mm) size masked incident light source and TF Mini Super measurement apparatus for multiple devices in a single substrate. The EQE system was calibrated with a Si photodiode before measurement. For the light intensity dependence measurements, AM 1.5 sunlight from a filtered Xenon lamp was adjusted by using a set of neutral density filters. UV-vis absorption spectra of polymers were measured on PerkinElmer Lambda 900 UV-vis/near-IR spectrophotometer. Atomic force microscopy (AFM) characterization of the surface morphology was done on the active layers of the actual polymer solar cells, used in the photovoltaic measurements, by using a Bruker Dimension scanning probe microscope (SPM) system.

4.3 Results and Discussions

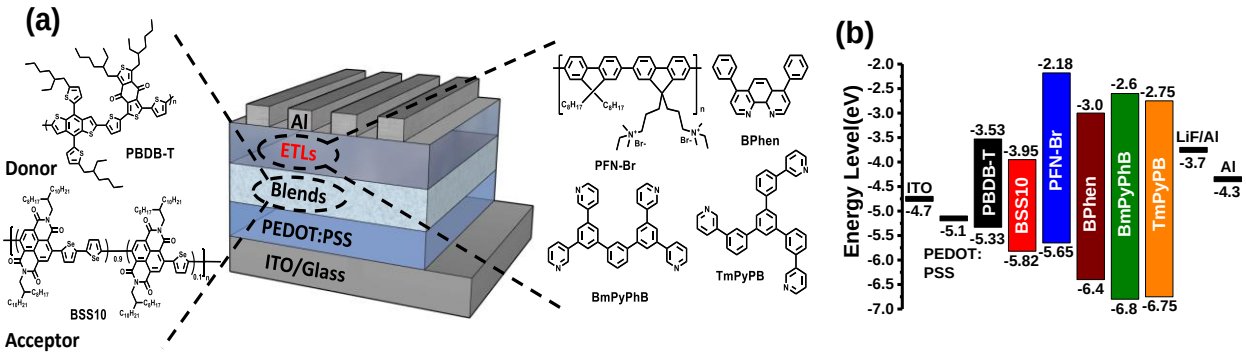

Figure 12. The conventional OPV device architecture with donor polymer PBDB-T and acceptor polymer BSS10 (a), Molecular structures of electron-transport materials, (c) Energy level diagram of the conventional all-PSC device with each electron-transport material.

The photovoltaic properties of all-PSCs with each ETL based on PBDB-T:BSS10 blends, which have complementary absorption as the active layer, were investigated. The conventional device (Figure 1a) with the structure: ITO/PEDOT:PSS/Blends/ELT/Al were fabricated and evaluated. On the basis of our previous work, we applied the optimized blend of active layer

composition and processing condition. The optimum donor and acceptor blend composition is 1:0.6 wt/wt and the active layer is thermally annealed at 175 °C for 10 min without any processing additives in the glove box. We firstly screened and optimized the solution-deposited BPhen ETL with a case of doped BPhen with an alkali metal salt (Cs_2CO_3) dopant co-dissolved in formic acid solution as a standard layer in this work. The photovoltaic parameters are provided in Table S1-S2. We found the optimal concentration of BPhen (24 mg/ml) and dopants concentration (10 wt%).

Table 6. Photovoltaic Properties of 1:0.6 wt/wt PBDB-T:BSS10 Blend All-Polymer Solar Cells with different electron-transport layers.

Cathode	J_{sc} (mA/cm^2)	V_{oc} (V)	FF	PCE_{max} (%)	PCE_{ave} (%)	Rs (Ωcm^2)	Rsh (Ωcm^2)
Al	12.99	0.79	0.49	5.57	5.02 (±0.34) [a]	18.9	474
LiF (1 nm)/Al	13.78	0.85	0.50	6.22	5.80 (±0.35) [a]	19.4	524
Formic Acid/Al	16.85	0.84	0.46	6.83	6.41 (±0.21) [a]	11.3	146
PFN-Br	15.50	0.86	0.55	7.92	7.34 (±0.32) [b]	9.4	391
BPhen/Al	17.96	0.85	0.48	8.14	7.33 (±0.47) [b]	10.5	166
BPhen +Cs_2CO_3 10 wt%/Al	18.37	0.85	0.48	8.53	7.57 (±0.45) [b]	10.3	170
BmPyPhB +Cs_2CO_3 10 wt%/Al	18.78	0.85	0.48	8.52	7.69 (±0.42) [b]	10.1	166
TmPyPB +Cs_2CO_3 10 wt%/Al	18.59	0.85	0.48	8.38	7.55 (±0.51) [b]	9.9	161

[a)] Average PCE values obtained from 10 separate devices. [b)] Average PCE values obtained from more than 15 separate devices.

Each ETL of all-PSCs show various photovoltaic properties. The corresponding photovoltaic parameters of all-PSCs are summarized in Table 1, and the current density (J_{sc})-voltage (V) curves and external quantum efficiency (EQE) are shown in Figure 2. First, all-PSCs in which only Al cathode was deposited without any ETMs as a control in this work showed lowest short-circuit current (J_{sc}) of 12.99 mA/cm^2 and open circuit voltage (V_{oc}) of 0.79. In contrast, the

thermally deposited Lithium fluoride (LiF) had improved J_{sc} of 13.70 mA/cm^2 with significantly enhanced V_{oc} of 0.85. It was already shown in many literatures that thin LiF (1 nm) layer lowered electron-extraction barrier by reducing the work function of the cathode. As compared to thermal evaporation case of LiF, solution-processed ETL under ~5 nm of PFN-Br (0.5 mg/ml) dissolved in Methanol improved the device performance significantly. All photovoltaic parameters are reinforced with Jsc of 15.57 mA/cm^2, V_{oc} of 0.86 and fill factor (FF) of 0.55 which make 7.36 % PCE_{avg}. We could assume that the enhancement of device performance from a PFN derivative PFN-Br ETL is because of strong interface dipole between ETL and metal electrode with better energy level alignment by lowering the high work-function of metal already known in the literature. Also, the dipole of the polymers formed the superposition of the built-in field could lead to the enhancement of V_{oc}. The small-molecule ETL of BPhen as standard in this report also showed enhanced device performance of 7.33% PCE_{avg} as compared to PFN-Br ETL case.

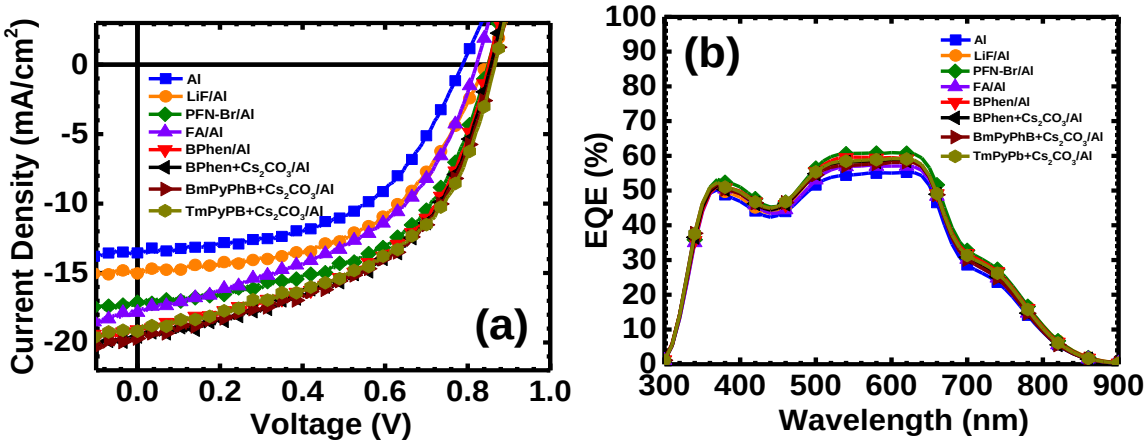

Figure 13. Current density (J_{sc})-Voltage (V) characteristics under AM 1.5G 100 mA/cm2 illumination (a) and EQE spectra (b) for optimal PBDB-T: BSS10 all-polymer solar cells with different electron-transport layers. The PBDB-T:BSS10 blend active layers were thermally annealed (175 °C,10 min).

However, the photovoltaic parameters of the devices showed a different trend with better J_{sc} of 17.89 mA/cm^2 and similar V_{oc} of 0.85, but with quite lowered FF of 0.48 than PFN-Br ETL. Furthermore, the incorporation of Cs_2CO_3 10 wt% in BPhen ETL resulted in even more improvement of J_{sc} of 18.48 mA/cm^2 of the devices. This result suggests that charge extraction is improved by the increased conductivity from the BPhen doped with alkali metal salt of Cs_2CO_3. Furthermore, we also identified that other small-molecule ETLs (BmPyPhB and TmPyPB) doped with Cs_2CO_3 10 wt% works well in all-PSCs with even higher J_{sc} of 18.78 mA/cm^2 and 18.59 mA/cm^2 respectively. EQE spectra of the all-PSCs with each ETL (Figure 2b) exhibited almost the same curve shape with well-matched absorption spectra of polymer blends. These results clearly show that the solution-processed new ETLs with the combination of alkali metal salt dopants are synergistic in improving the performance of all-PSCs and promising for further study of a new ETLs for all-PSCs.

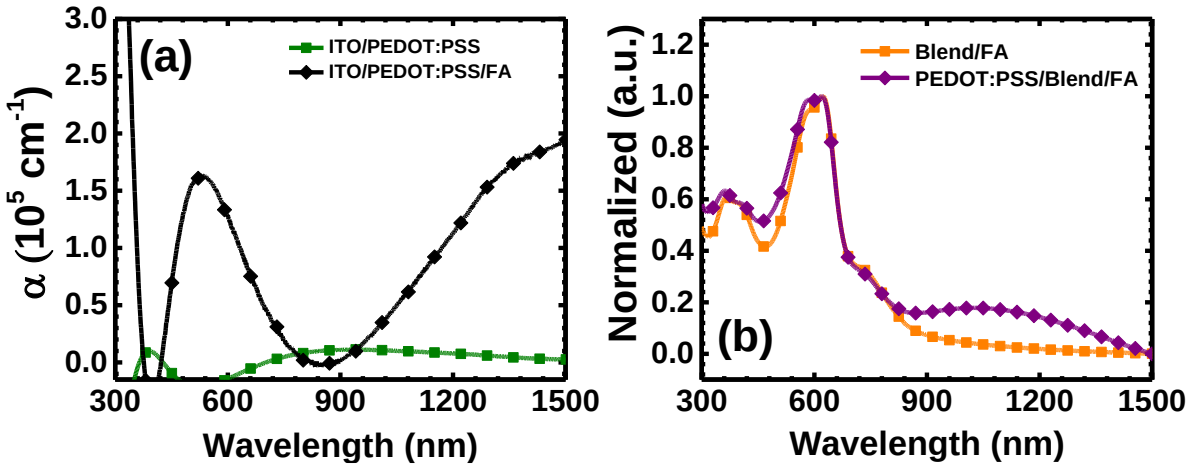

Figure 14. (a) Thin-film optical absorption spectra of the PEDOT:PSS and PEDOT:PSS with the formic acid layer. (b) Optical absorption spectra of PBDB-T:BSS10 blend with different interlayers

It is noteworthy that at the very beginning when we made the all-PSC devices from the all-new ETLs dissolved in formic acid, we observed untrue high photocurrent shown in Figure S1 and Table S3. First of all, there have been many studies that people have tried to modify the PEDOT:PSS film to enhance the electrical properties by adding various organic solvents, salts, acids, and surfactants.[27,29–31] In those studies, this phenomenon has also already observed in the literature that the modified PEDOT:PSS with [HOEMIm]-[HSO4] showed unreal high Jsc value.[26] The modified PEDOT:PSS with high in-plane conductivity made the device possess more carriers in a larger area, and these increased carriers under illumination without an aperture mask could cause the fake high value of the photocurrent.[26] To get rid of this problem, we tried to remove all the surrounded spin-coated layers between each device and whole device substrates by using a cotton swap. After applying this method, we corrected the real photocurrent values of the all-PSCs. Also, we observed that the shifted spectrum and improved absorption (Figure 3) after 900 nm when we made a spin-coated formic acid layer on top of the PEDOT:PSS film. Furthermore, we conducted a conductivity measurement by the four-point probe for pristine thin film PEDOT:PSS and PEDOT:PSS with the spin-coated formic acid layer. While the conductivity of pristine thin film PEDOT:PSS is 0.003 S/cm, PEDOT:PSS treated by formic acid spin coating shows 0.07 S/cm, which is more than one order of magnitude increase. Obviously, these results suggest that formic acid causes the doped situation of PEDOT:PSS. We also made devices and investigated photovoltaic performance (Table 1) from the only spin-coated formic acid layer on top of the blend. These devices showed higher J_{sc} of 16.85 mA/cm^2 than PFN-Br ETL devices. This interaction of formic acid with PEDOT:PSS in all-PSCs suggests that formic acid solution can make the PEDOT:PSS film more conductive and help to get improved J_{sc} in all-PSCs.

We investigated the charge collection probability P (E, T) under short-circuit condition to understand the influence of each ETL.[32–34] Since this value was calculated by the short-circuit current densities under dark and illumination conditions, the reduced FF and increased shunt resistance (Rsh) from new-ETLs caused the lowered charge collection probability than Al, LiF/Al, and PFN-Br ETL/Al is shown in Table S5. The short-circuit current density as a function of an illumination intensity (P_{light}) was measured to understand the charge recombination kinetics of the devices.[35] The linearity (α=1) of the power-law dependence of J_{sc} on P_{light} ($J_{sc} \propto (P_{light})^{\alpha}$) indicates the weak carrier loss from bimolecular recombination. New-ETLs which showed low FF reflected the more off linearity as compared to the PFN-Br ETL. These results can point out that the high recombination probability based on low fill factor from new-ETLs would be one of the problems and should be investigated deeply from future study.

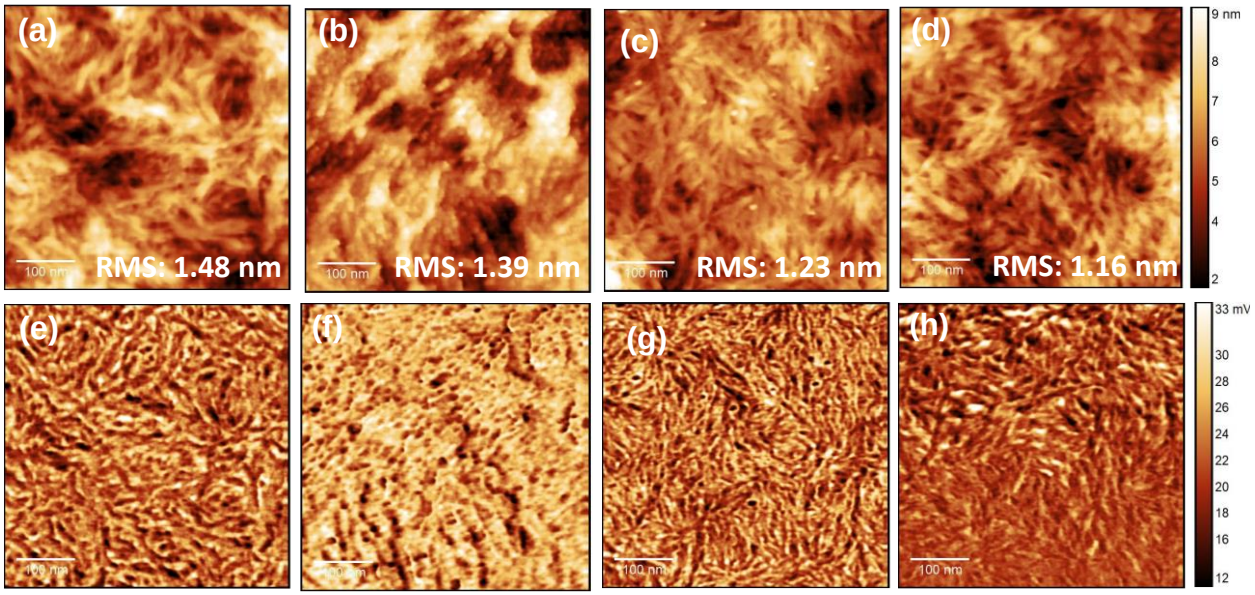

Figure 15. AFM height (a, b, c, and d) and phase (e, f, g, and h) images (500 nm x 500 nm) of the surfaces of PBDB-T:BSS10 (a, e), PBDB-T:BSS10 with PFN-Br layer (b, f) , PBDB-T:BSS10 with Formic acid layer (c, g) and PBDB-T:BSS10 with BPhen layer dissolved in formic acid (d, h).

To understand the surface morphology of film from new-ETLs on top of the blend, atomic force microscopy (AFM) was carried out. The height and phase images of the blend films without and with each ETL are presented in Figure 4, S2. We obviously observed the changes of surface roughness by taking the root-mean-square (RMS) values from each sample. The case of Al cathode without ETL showed the highest RMS value (1.48 nm) and PFN-Br ETL had a little smooth surface with RMS (1.39 nm). Interestingly, the roughness started to be reduced a lot with the formic acid layer to 1.23 nm and became smoother surface within the range of 1.0 ~ 1.2 nm as with new-ETLs. This results can partly explain the smoother surface can help to form the proper interface contact and stimulate the electron extraction through the interfaces to help to get high photocurrent.

4.4 CONCLUSIONS

We have shown new solution-processed ETLs can enhance photocurrent in all-PSCs. Furthermore, the doped ETLs of BPhen, BmPyPhB, and TmPyPB with 10 wt % alkali metal salt (Cs_2CO_3) resulted in significantly high J_{sc} of 18.37 mA/cm^2, 18.78 mA/cm^2, and 18.59 mA/cm^2 respectively. We also found the formic acid as a solvent for ETMs can form the doped PEDOT:PSS film without any damage for the active layer, leading to slightly increased J_{sc} of 16.85 mA/cm^2 as compared to PFN-Br ETL. Studies of surface morphologies from AFM with each ETL revealed that more smooth surface roughness can be formed by solution processed new-ETLs, which could help to get better contact between ELTs and electrode. We expect these results could boost to develop more effective ETLs for high-performance all-PSCs.

4.5 REFERENCES

(1) Chiang, C. K.; Fincher, C. R.; Park, Y. W.; Heeger, A. J.; Shirakawa, H.; Louis, E. J.; Gau, S. C.; MacDiarmid, A. G. Electrical Conductivity in Doped Polyacetylene. *Phys. Rev. Lett.* **1977**, *39* (17), 1098–1101.

(2) Forrest, S. R.; Thompson, M. E. Introduction: Organic Electronics and Optoelectronics. *Chem. Rev.* **2007**, *107* (4), 923–925.

(3) Brédas, J.-L.; Norton, J. E.; Cornil, J.; Coropceanu, V. Molecular Understanding of Organic Solar Cells: The Challenges. *Acc. Chem. Res* **2009**, *42* (11).

(4) Zhou, N.; Facchetti, A. Naphthalenediimide (NDI) Polymers for All-Polymer Photovoltaics. *Mater. Today* **2018**, *21* (4), 377–390.

(5) Huang, Y.; Kramer, E. J.; Heeger, A. J.; Bazan, G. C. Bulk Heterojunction Solar Cells: Morphology and Performance Relationships. *Chem. Rev.* **2014**, *114* (14), 7006–7043.

(6) Lu, L.; Zheng, T.; Wu, Q.; Schneider, A. M.; Zhao, D.; Yu, L. Recent Advances in Bulk Heterojunction Polymer Solar Cells. **2015**.

(7) Zhan, C.; Zhang, X.; Yao, J. New Advances in Non-Fullerene Acceptor Based Organic Solar Cells. *RSC Adv.* **2015**, *5* (113), 93002–93026.

(8) Yan, H.; Chen, Z.; Zheng, Y.; Newman, C.; Quinn, J. R.; Dötz, F.; Kastler, M.; Facchetti, A. A High-Mobility Electron-Transporting Polymer for Printed Transistors. *Nature* **2009**, *457* (7230), 679–686.

(9) Fabiano, S.; Himmelberger, S.; Drees, M.; Chen, Z.; Altamimi, R. M.; Salleo, A.; Loi, M. A.; Facchetti, A. Charge Transport Orthogonality in All-Polymer Blend Transistors, Diodes, and Solar Cells. *Adv. Energy Mater.* **2014**, *4* (6), 1–7.

(10) Courtright, B. A. E.; Jenekhe, S. A. Polyethylenimine Interfacial Layers in Inverted Organic

Photovoltaic Devices : E Ff Ects of Ethoxylation and Molecular Weight on E Ffi Ciency and Temporal Stability. **2015**, 1–5.

(11) Chen, L. M.; Xu, Z.; Hong, Z. R.; Yang, Y. Interface Investigation and Engineering - Achieving High Performance Polymer Photovoltaic Devices. *J. Mater. Chem.* **2010**, *20* (13), 2575–2598.

(12) Steim, R.; Kogler, F. R.; Brabec, C. J. Interface Materials for Organic Solar Cells. *J. Mater. Chem.* **2010**, *20* (13), 2499.

(13) Yi, C.; Hu, X.; Gong, X.; Elzatahry, A. Interfacial Engineering for High Performance Organic Photovoltaics. *Mater. Today* **2016**, *19* (3), 169–177.

(14) Zeng, H.; Zhu, X.; Liang, Y.; Guo, X. *Interfacial Layer Engineering for Performance Enhancement in Polymer Solar Cells*; 2015; Vol. 7.

(15) Duan, C.; Zhang, K.; Zhong, C.; Huang, F.; Cao, Y. Recent Advances in Water/Alcohol-Soluble π-Conjugated Materials: New Materials and Growing Applications in Solar Cells. *Chem. Soc. Rev.* **2013**, *42* (23), 9071–9104.

(16) Yang, T.; Wang, M.; Duan, C.; Hu, X.; Huang, L.; Peng, J.; Huang, F.; Gong, X. Inverted Polymer Solar Cells with 8.4% Efficiency by Conjugated Polyelectrolyte. *Energy Environ. Sci.* **2012**, *5* (8), 8208.

(17) Hu, Z.; Zhang, K.; Huang, F.; Cao, Y. Water/Alcohol Soluble Conjugated Polymers for the Interface Engineering of Highly Efficient Polymer Light-Emitting Diodes and Polymer Solar Cells. *Chem. Commun.* **2015**, *51* (26), 5572–5585.

(18) Li, C.; Schwab, M.; Zhao, Y.; Chen, L.; Bruder, I.; Münster, I.; Erk, P.; Müllen, K. A Phenanthroline Derivative as Exciton Blocking Material for Organic Solar Cells. *Dye. Pigment.* **2013**, *97* (1), 258–261.

(19) Liu, X.; Wu, Y.; Li, X.; Zhang, W.; Zhao, L.; Wang, H. Q.; Fang, J. CdS-Phenanthroline Derivative Hybrid Cathode Interlayers for High Performance Inverted Organic Solar Cells. *J. Mater. Chem. A* **2015**, *4* (1), 297–302.

(20) Chang, C. C.; Lin, C. F.; Chiou, J. M.; Ho, T. H.; Tai, Y.; Lee, J. H.; Chen, Y. F.; Wang, J. K.; Chen, L. C.; Chen, K. H. Effects of Cathode Buffer Layers on the Efficiency of Bulk-Heterojunction Solar Cells. *Appl. Phys. Lett.* **2010**, *96* (26), 94–97.

(21) Farinhas, J.; Ferraria, A. M.; do Rego, A. M. B.; Morgado, J.; Charas, A. Understanding the Role of Phenanthroline as Interlayer in Bulk Heterojunction Organic Photovoltaic Cells. *ChemistrySelect* **2016**, *1* (18), 5638–5646.

(22) Earmme, T.; Jenekhe, S. A. High-Performance Multilayered Phosphorescent OLEDs by Solution-Processed Commercial Electron-Transport Materials. *J. Mater. Chem.* **2012**, *22* (11), 4660–4668.

(23) Earmme, T.; Jenekhe, S. A. Improved Electron Injection and Transport by Use of Baking Soda as a Low-Cost, Air-Stable, n-Dopant for Solution-Processed Phosphorescent Organic Light-Emitting Diodes. *Appl. Phys. Lett.* **2013**, *102* (23).

(24) Earmme, T.; Jenekhe, S. A. Solution-Processed, Alkali Metal-Salt-Doped, Electrona Transport Layers for High-Performance Phosphorescent Organic Light-Emitting Diodes. *Adv. Funct. Mater.* **2012**, *22* (24), 5126–5136.

(25) Ahmed, E.; Earmme, T.; Jenekhe, S. A. New Solution-Processable Electron Transport Materials for Highly Efficient Blue Phosphorescent OLEDs. *Adv. Funct. Mater.* **2011**, *21* (20), 3889–3899.

(26) Huang, L.; Cheng, X.; Yang, J.; Zhang, L.; Zhou, W.; Xiao, S.; Tan, L.; Chen, L.; Chen, Y. High-Performance Polymer Solar Cells Realized by Regulating the Surface Properties of

PEDOT:PSS Interlayer from Ionic Liquids. *ACS Appl. Mater. Interfaces* **2016**, *8* (40), 27018–27025.

(27) Mengistie, D. A.; Ibrahem, M. A.; Wang, P. C.; Chu, C. W. Highly Conductive PEDOT:PSS Treated with Formic Acid for ITO-Free Polymer Solar Cells. *ACS Appl. Mater. Interfaces* **2014**, *6* (4), 2292–2299.

(28) Walzer, K.; Männig, B.; Pfeiffer, M.; Leo, K. Highly Efficient Organic Devices Based on Electrically Doped Transport Layers. *Chem. Rev.* **2007**, *107* (4), 1233–1271.

(29) Zhao, Z.; Wu, Q.; Xia, F.; Chen, X.; Liu, Y.; Zhang, W.; Zhu, J.; Dai, S.; Yang, S. Improving the Conductivity of PEDOT:PSS Hole Transport Layer in Polymer Solar Cells via Copper(II) Bromide Salt Doping. *ACS Appl. Mater. Interfaces* **2015**, *7* (3), 1439–1448.

(30) Huang, L.; Cheng, X.; Yang, J.; Zhang, L.; Zhou, W.; Xiao, S.; Tan, L.; Chen, L.; Chen, Y. High-Performance Polymer Solar Cells Realized by Regulating the Surface Properties of PEDOT : PSS Interlayer from Ionic Liquids. **2016**.

(31) Mcgillivray, D.; Thomas, J. P.; Abd-ellah, M.; Heinig, N. F.; Leung, K. T. Performance Enhancement by Secondary Doping in PEDOT:PSS/ Planar-Si Hybrid Solar Cells. **2016**, 6–11.

(32) Fan, B.; Ying, L.; Wang, Z.; He, B.; Jiang, X.-F.; Huang, F.; Cao, Y. Optimisation of Processing Solvent and Molecular Weight for the Production of Green-Solvent-Processed All-Polymer Solar Cells with a Power Conversion Efficiency over 9%. *Energy Environ. Sci.* **2017**, *10* (5), 1243–1251.

(33) Mihailetchi, V. D.; Xie, H.; De Boer, B.; Koster, L. J. A.; Blom, P. W. M. Charge Transport and Photocurrent Generation in Poly(3-Hexylthiophene): Methanofullerene Bulk-Heterojunction Solar Cells. *Adv. Funct. Mater.* **2006**, *16* (5), 699–708.

(34) Fan, B.; Ying, L.; Zhu, P.; Pan, F.; Liu, F.; Chen, J.; Huang, F.; Cao, Y. All-Polymer Solar Cells Based on a Conjugated Polymer Containing Siloxane-Functionalized Side Chains with Efficiency over 10%. *Adv. Mater.* **2017**, *29* (47), 1–7.

(35) Hwang, Y.; Courtright, B. A. E.; Ferreira, A. S.; Tolbert, S. H.; Jenekhe, S. A. 7 . 7 % Effi Cient All-Polymer Solar Cells. **2015**, 4578–4584.

Chapter 5. CONCLUSIONS AND OUTLOOK

5.1 CONCLUSIONS

Throughout this work, I investigated factors that affect the performance of all-polymer solar cells (all-PCSs) based on naphthalene diimide-biselenephene copolymer acceptors. Although there are many challenges in this research field of organic photovoltaics (OPVs), specifically I focused on the study of all-PCSs regarding optimal photovoltaic properties, blend morphology, and cathode interfacial engineering.

I studied inverted all-PSCs based on naphthalene diimide-biselenophene copolymer acceptor bearing 2-octyldodecyl side chains (PNDIBS). Systematic optimization process for inverted all-PCSs was conducted to low-Mn PNDIBS (LP, Mn=28.4 kDa) and high-Mn PNDIBS (HP, Mn=53.7 kDa) with donor polymer PBDB-T, which has complementary absorption spectrum. In the process of optimization of all-PCSs with LP and HP, thermally annealed PBDB-T: HP blend devices with processing additive showed PCE of 9.4 % with J_{sc} of 18.32 mA/cm^2. In contrast, PBDB-T: LP blend devices with processing additive had PCE of 7.9% when they are dried at room temperature. Besides, HP shows enhanced electron mobility, greater face-on molecular orientation and more balanced charge transport from SCLC and 2D-GIWAXS characterization of active layers from the all-PCSs.

In addition, to further explore the effects of controlling bulk crystallinity in all-PCSs with their photovoltaic properties and blend morphology, a series of new naphthalene diimide (NDI)-biselenophene (BS) / NDI-selenophene (S) random copolymer acceptors BSS*x* (*x*=10, 20, and 50) whose crystallinity varies with NDI-selenophene composition, were investigated in all-PCSs. With the enhanced absorption, bulk electron mobility and reduced crystallinity of BSS10 and BSS20 acceptor, PBDB-T: BSS10 and PBDB-T: BSS20 blend devices showed high photovoltaic

performance with PCE of 9.5% with J_{sc} of 20.02 mA/cm^2 and 9.6% with J_{sc} of 19.70 mA/cm respectively. This miscible blend of PBDB-T:BSS10 and BSS20 have favorable morphology with reduced domain sizes, improved face-on orientation, and more balanced charge transport as compared to PBDB-T:BSS0 blend where BSS0 consists of 0% of NDI-selenophene polymer backbone as reference polymer acceptor. Also, these all-PCSs were achieved with facile thermal annealing without any processing additives and the PBDB-T: BSS20 blend devices even can maintain the high performance of PCE above 8% with active layer thermally annealed at 200 ℃.

Finally, I investigated the cathode interface with solution processable electron transport materials (BPhen, BmPyPhB, and TmPyPB) in conventional PBDB-T:BSS10 blend device. In this study, I observed solution-processed electron transport layers (ETLs) with alkali metal salt dopants can be applied to all-PCSs. Those ETLs shows superior performance in photocurrent (~18 mA/cm^2) from a systematic study with different cases of the cathode. Although relatively low fill factor of this system is remaining a task for the overall improvement of all-PCSs with solution-processed ETLs, this work can highlight the importance of engineering cathode interface for developing high-performance all-PCSs with solution processable interlayers. Overall, the results of this study have helped to advance the field of OPVs. In particular, this work provides an additional guideline to develop enhanced performance all-PCSs for the next generation of organic electronic devices. Further investigation should be continued to expand our knowledge and to advance the technology in this field with deeper understanding.

5.2 OUTLOOK

Research on organic photovoltaics (OPVs) is an ongoing and attractive topic in both academia and industry. From these studies, all-polymer solar cells (all-PSCs) based on naphthalene

diimide-biselenophene copolymer acceptors can show a bright future for high-performance all-PCSs as compared to other all-PCSs or fullerene based polymer solar cells. However, relative low fill factor in this system of all-PSCs, which is dominated by blend morphology and is interrelated with recombination process, remains an unsettled question. Since all-PCSs is based on mixing the donor polymer and acceptor polymer as bulk heterojunction structure to obtain increased interface for efficient charge separation within a limited diffusion length of excitons, obtaining an optimal blend morphology is a crucial key for best photovoltaic performance. Certainly, it is thus necessary to understand polymer blends morphology and kinetics and develop optimal device engineering for each system of all-PSCs.

Besides, laboratory scale fabrication and industrial scale or commercialization for all-PCSs would be a different story. Film morphology and stacked interlayers of devices from spin coating technique would be safe from some defects or formation of consistent blend morphology due to a millimeter device of laboratory scale. However, this laboratory scale technique would have limitations such as inconsistent film morphology with partly different thickness and increased defects on large device area. Moreover, deformation of blend morphology when they are applied on top of the flexible substrate, thermal stability, and oxidation of organic devices should be considered for future application. Currently, the roll-to-roll process technique or blade coating process for large-scale production has been tried and desired for further developments of this field.